a biochemical analysis of tau proteins in the white matter from patients with PDC was carried out to elucidate whether these TFGs are biochemically different from other tau-positive constituents.

MATERIALS AND METHODS

Cases

The present study was carried out using brains taken at autopsy from patients with PDC (n = 35), Guamanian PDC with amyotrophic lateral sclerosis (ALS; n = 4), Guamanian ALS (n = 7), Guamanian nonPDC, nonALS controls with neurologic disorders (n = 11), CBD (n = 10), PSP (n = 15), Pick disease (n = 4), AD (n = 10), AGD (n = 5), and myotonic dystrophy (n = 5; Table). Myotonic dystrophy was known to have NFTs in the neocortex and in subcortical nuclei (7). All of the Guamanian cases were examined and their condition diagnosed clinicopathologically by the authors (8–13). Some of the clinical and neuropathologic findings of the cases of CBD, PSP, Pick disease, AD, AGD, and myotonic dystrophy have already been reported elsewhere (14–26).

Histochemistry and Immunohistochemistry

The frontal white matter from autopsied brain tissue was cut into blocks, fixed in formalin, embedded in paraffin, and then sectioned at 4 μm. Some of these sections were stained with hematoxylin and eosin and by the Klüver-Barrera and Gallyas-Braak methods. The remaining sections were incubated with one of the following primary antibodies: anti-tau (AT8, monoclonal, 1:1000; Innogenetics, Temse, Belgium), anti-human tau (a gift from Professor Ihara, 1:1000; [27]), anti-ubiquitin (polyclonal, rabbit, 1:1000; Dako), and anti-glial fibrillary acidic protein (GFAP, polyclonal, rabbit, 1:1000; Dako). The immunolabeled sections were observed with the aid of a fluorescence microscope combined with a laser confocal system (TCS-SP; Leica, Heidelberg, Germany). For double immunostaining with anti-paired helical filaments (PHF) tau monoclonal (AT8, 1:1000; Innogenetics) and anti-GFAP/anti-ubiquitin/anti-phosphorylated neurofilaments (SMI31) antibodies, the specimens were blocked with nonimmune sera from horse or goat, depending on the secondary antibody used. Sections were first incubated with a mixture of the 2 primary antibodies and then with the fluorescence-labeled secondary antibodies (i.e. anti-mouse IgG coupled with fluorescein isothiocyanate [1:200; Cappel, Irvine, CA] and anti-rabbit IgG coupled with rhodamine [1:200; Cappel]).

TABLE. Summary of Cases Examined in This Study

Disease	Number	Gender of Cases	Age (years)
PDC of Guam (died 1979–1982)	35	23 male/2 female	64.4 ± 8.32
Guam PDC-ALS	4	2 male/2 female	63.0 ± 6.06
Guam ALS	7	3 male/4 female	52.1 ± 10.0
Guam control	11	4 male/7 female	68.8 ± 11.5
Corticobasal degeneration	10	4 male/6 female	65.7 ± 5.43
Progressive supranuclear palsy	15	8 male/7 female	74.4 ± 8.82
Pick disease	4	2 male/2 female	71.5 ± 3.70
Alzheimer disease	10	1 male/9 female	74.6 ± 15.1
Argyrophilic grain disease	5	3 male/2 female	82.4 ± 7.92
Myotonic dystrophy	5	3 male/2 female	54.4 ± 19.7

PDC, Parkinsonism–dementia complex; ALS, amyotrophic lateral sclerosis.

Quantitative Examination of Neurofibrillary Tangles and Tau-Positive Fine Granules

We performed quantitative analyses on the frontal subcortical white matter of brains from clinically diagnosed patients with PDC. The relationship between NFTs and TFGs was clarified by calculating the density of NFTs and TFGs in the frontal cortex of 12 patients with PDC. These 12 patients were sampled randomly from the 35 PDC cases examined in this study. With the aid of Gallyas-Braak staining, we computed the density of NFTs, including pretangles, in all layers of the 100-μm-wide frontal cortical ribbon. The number of TFGs in the center of the centrum semiovale in the frontal white matter was calculated by summing the number of TFGs in evenly distributed serial fields measuring 2.5 μm × 2.5 μm (giving a total area of 6.25 μm^2). The correlation between the density of NFTs and that of TFGs was estimated using Spearman's rank correlation coefficient. We used the Kruskal-Wallis test for comparing the density of NFTs with that of TFGs. Differences at $p < 0.05$ were considered significant.

Immunoelectron Microscopy

Paraffin-embedded, 6-μm-thick sections from the cerebral frontal white matter of PDC cases with tau-positive TFGs were immunostained with anti-tau antibody (AT8). The immunolabeling was visualized with diaminobenzidine (DAB), like for light microscope immunohistochemistry, and then processed for immunoelectron microscopy. After being post-fixed in 4% OsO_4 for 15 minutes, the sections were dehydrated in a graded ethanol series, embedded in epon 812, and then polymerized at 60°C for 24 hours. Ultrathin sections were cut and then stained with 3% lead acetate for 2 minutes and viewed with an electron microscope (H-9000; Hitachi, Japan) (28).

Biochemical Analysis

Frozen brain tissues from the frontal region, including both the gray matter and deep white matter of 4 PDC cases, one Guamanian ALS case with abundant TFGs in both the gray and white matter, one Guamanian control case, and 2 classic AD cases, were used for biochemical analysis. All of these brains were frozen at autopsy at –80°C. The gray and white matters were separated from each other macroscopically. Sarkosyl-insoluble tau was prepared according to a modification of the method of Goedert et al (29). Tissues were homogenized in a 10-fold (v/w) dilution of extraction buffer (10 mM Tris-HCl [pH 7.5], 1 mM EGTA, 0.8 M NaCl, 10% sucrose) and centrifuged at 23,000 × *g* for 20 minutes at 4°C. The pellets were rehomogenized in extraction buffer. Both of the 23,000 × *g* supernatants were combined, brought to 1% sarkosyl, and incubated for 1 hour at room temperature. After centrifugation at 113,000 × *g* for 20 minutes at 25°C, the

pellets were resuspended in 7 M guanidine-HCl and then dialyzed overnight against 30 mM Tris-HCl (pH 8.8). Dephosphorylation and immunoblotting were performed as described previously (30).

RESULTS

Microscope Study

The cerebral white matter of most patients with PDC exhibited no evident pallor with Kluver-Barrera stain. In addition to the TFGs, in the white matter of PDC (Fig. 1A, C), we found some tau-positive argyrophilic threads and coiled bodies. Some tiny tau-positive granular or thread-like structures with a diameter of 1 to 3 μm were also found in the PDC brains and in those of the other tauopathies studied here (Fig. 1B, D). These thread-like structures were found mainly in the frontal and temporal white matter and were not specific to PDC. They were also observed in the white matter of brains from patients with the other tauopathies examined in this study (AGD and CBD brain) and were clearly distinct from TFGs (Fig. 2A, B).

We observed TFGs in the frontal white matter of 30 of 35 patients with PDC (86%) and in 3 of 4 patients with PDC-ALS (75%). Moreover, only one of 7 Guamanian patients with ALS (14%) and 2 of 11 Guamanian controls (18%) whose cerebral cortices exhibited many NFTs also exhibited TFGs (Fig. 3). However, no TFGs were found in the brains of patients with myotonic dystrophy, Pick disease, or AD. In CBD brains, we found large numbers of argyrophilic threads and coiled bodies, but no TFGs (Fig. 2B). The TFGs were globe-shaped and approximately 3 to 6 μm in diameter, and were distinct from argyrophilic threads. TFGs were positive to both AT8 and anti-human tau antibodies (Fig. 1A, B), but some parts of them were not stained by the Gallyas-Braak method. Some TFGs consisted of globular dense tau-positive structures surrounded by weakly tau-positive fluffy materials (Fig. 1C). They were observed frequently in the frontal white matter, the frontal lobe, and the temporal subcortical white matter. In the PDC cases in which TFGs were abundant in the frontal white matter, some were also found in the frontal cortex. However, TFGs were only rarely observed in the spinal cord, cerebellum, or brainstem.

Confocal scanning microscope observations of immunofluorescence double-labeled sections showed that GFAP and phosphorylated neurofilament were not localized on TFGs (Fig. 4A, B). Although most of the TFGs exhibited no colocalization of ubiquitin and tau, it was observed on some (Fig. 4C). The pattern of this colocalization, when it was observed, varied from only a small part (i.e. the center) of the TFG to staining in almost all of it.

Quantitative Analysis of Tau-Positive Fine Granules and Neurofibrillary Tangles

We found no significant relationship between the number of NFTs and the number of TFGs. However, the 12 patients with PDC could be divided into 2 groups: those with more than 200 NFTs/100 μm-length of the frontal cortical ribbon and those with less (Fig. 5). The graph shown in Figure 4 shows that TFGs were only observed in those PDC cases with more than approximately 200 NFTs/100 μm-length of the frontal cortical ribbon. There was no significant

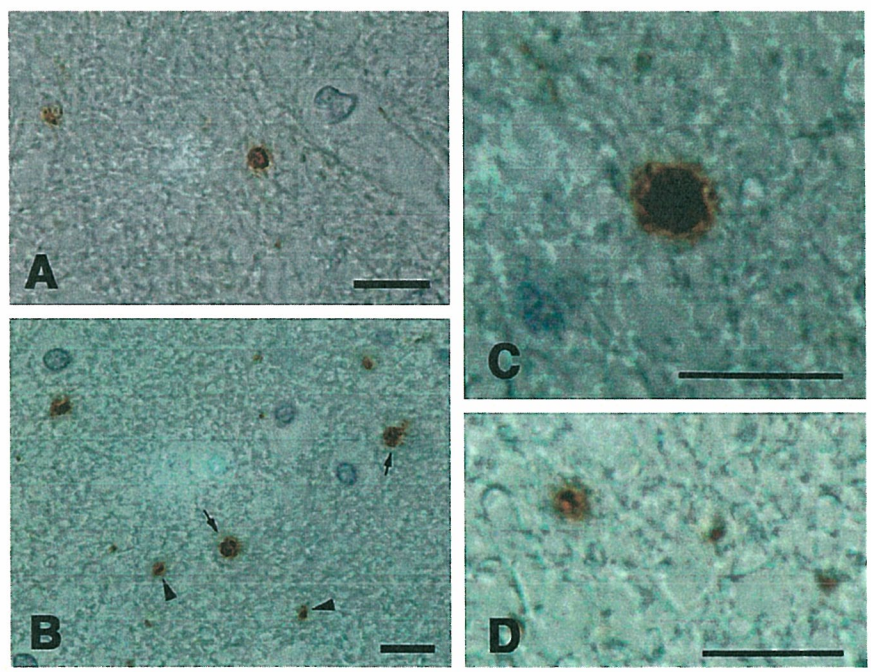

FIGURE 1. Immunohistochemical findings in the frontal white matter of parkinsonism–dementia complex of Guam (PDC) brains. Anti-tau antibodies (human tau **[A]** and AT8 **[B]**) were used to examine sections of the frontal white matter. **(B)** Tau-positive fine granules (TFGs) (arrows) are globe-shaped and approximately 3 to 6 μm in diameter, and are distinct from argyrophilic threads. They were observed frequently in the frontal white matter. Tiny tau-positive granular structures (arrowheads) of 1 to 3 μm in diameter were found in the PDC brains and those of other tauopathies. These structures are thus not specific to PDC and could be clearly distinguished from TFGs. High-power views of TFGs **(C)** and tiny tau-positive granular structures **(D)**, both stained immunohistochemically for tau using AT8. **(C)** Some TFGs consisted of globular dense tau-positive structures surrounded by weakly tau-positive fluffy materials. Scale bars: 10 μm.

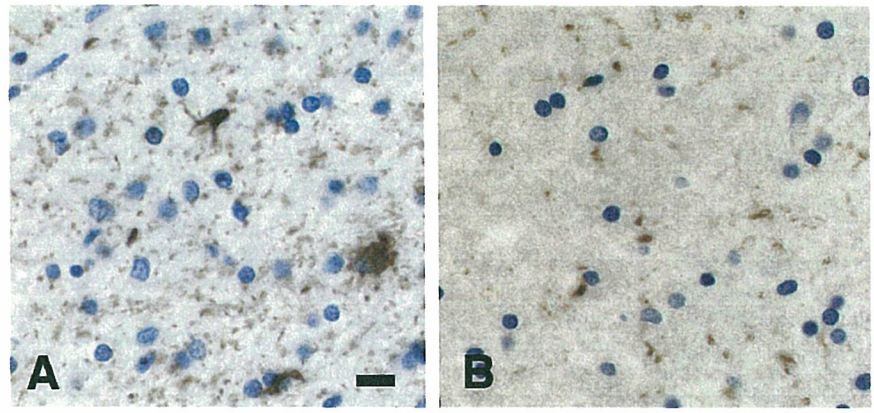

FIGURE 2. Immunohistochemical findings in the frontal white matter of brains with argyrophilic grain disease (AGD) **(A)** and corticobasal degeneration (CBD) **(B)** using anti-tau (AT8) antibody. Abundant tiny tau-positive granular structures were found, but no tau-positive fine granules were observed found in the frontal white matter of brains with AGD **(A)** and CBD **(B)**. Scale bars: 10 μm.

correlation between the degree of white matter degeneration and the density of TFGs.

Immunoelectron Microscope Observations

Most of the AT8-positive TFGs had some contact with the myelin outer loop, but no TFGs were observed within the myelin sheath or the axons (Fig. 6A). High-power views of these sections revealed that TFGs contained round structures that were 20 to 30 nm in diameter (including the DAB substrate) (Fig. 6B). These structures were also observed near the nucleus of glial cells that were thought to be oligodendroglia (Fig. 6C, D).

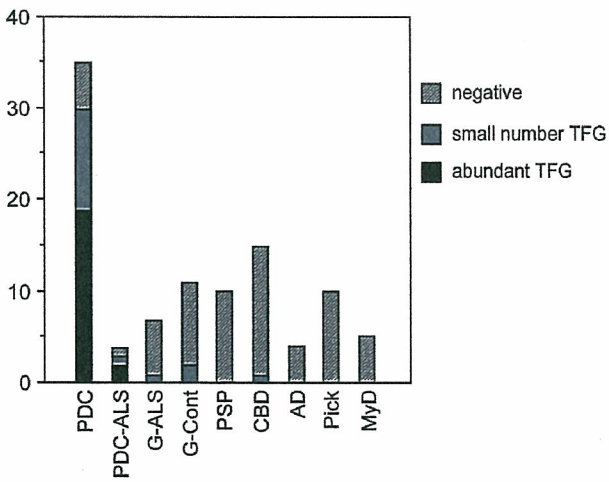

FIGURE 3. Tau-positive fine granules (TFGs) in the frontal white matter of brains with various tauopathies. Histogram showing the number of the cases having abundant TFGs (black), cases with only a small number of TFGs (narrow slash mark), and TFG-negative cases (broad slash mark) in each disease group. The density 50 TFGs/100 μm^2 marked the border between the "abundant TFGs" group and the "small number of TFGs" group. PDC, Parkinsonism–dementia complex; G-ALS, Guam amyotrophic lateral sclerosis; G-Cont, Guam control; CBD, corticobasal degeneration; PSP, progressive supranuclear palsy; AD, Alzheimer disease; Pick, Pick disease; MyD, myotonic dystrophy.

Biochemical Analysis

The sarkosyl-insoluble fraction prepared from the white matter of the frontal lobes of PDC cases that exhibited TFGs were analyzed by Western blotting with a the phosphorylation-independent anti-tau antibody HT-7. Two major bands were detected, one with an apparent molecular mass of 60 kDa and another of 64 kDa, and one minor band with an apparent molecular mass of 68 kDa. After dephosphorylation, these bands appeared as one major band corresponding to a 4-repeat tau isoform with zero amino acid inserts (4R0N) and 3 minor bands corresponding to a 4-repeat tau isoform with 29 amino acid inserts (4R29N), a 3-repeat tau isoform with zero amino acid inserts (3R0N), and a 3-repeat tau isoform with 29 amino acid inserts (3R29N; Fig. 7).

The insoluble tau extracted from the gray matter of cortices from the PDC cases resolved into 3 bands of apparent molecular mass 60, 64, and 68 kDa. Six bands were detected after dephosphorylation, corresponding to 6 tau isoforms that resembled those that were resolved in AD brains. Similar results were obtained from the analysis of another PDC case (PDC-4) and one Guamanian ALS case with abundant TFGs (data not shown). No insoluble tau was extracted from the frontal brain of a Guamanian control. Accumulations of both 3R and 4R tau isoforms were detected in the white matter of the PDC cases. However, when compared with tau in the gray matter, the levels of 4R tau isoforms were high and the levels of 3R tau isoforms were very low, which was different from those in the gray matter in which similar levels of 3R and 4R tau isoforms or slightly higher levels of 3R tau isoforms were detected. Furthermore, the 4R tau band pattern after dephosphorylation was most obvious in cases in which TFGs were abundant in the white matter. These results suggest that the TFGs in the white matter in the patients with PDC were composed predominantly of 4R tau isoforms.

Sarkosyl-insoluble tau from the white matter of AD brains consisted of a triplet of apparent molecular mass 60, 64, and 68 kDa, which resolved into 6 bands after dephosphorylation (data not shown), indicating that in AD, the tau isoforms deposited in the white matter (mostly in axons) were the same as those deposited in the gray matter, although there was far less of the pathologic tau in the white matter than in the gray matter.

DISCUSSION

TFGs are novel and unique tau-positive inclusions that we observed in the frontal white matter of 86% of the patients with PDC examined here. No TFGs were found in the brains of patients with myotonic dystrophy, Pick disease, or AD.

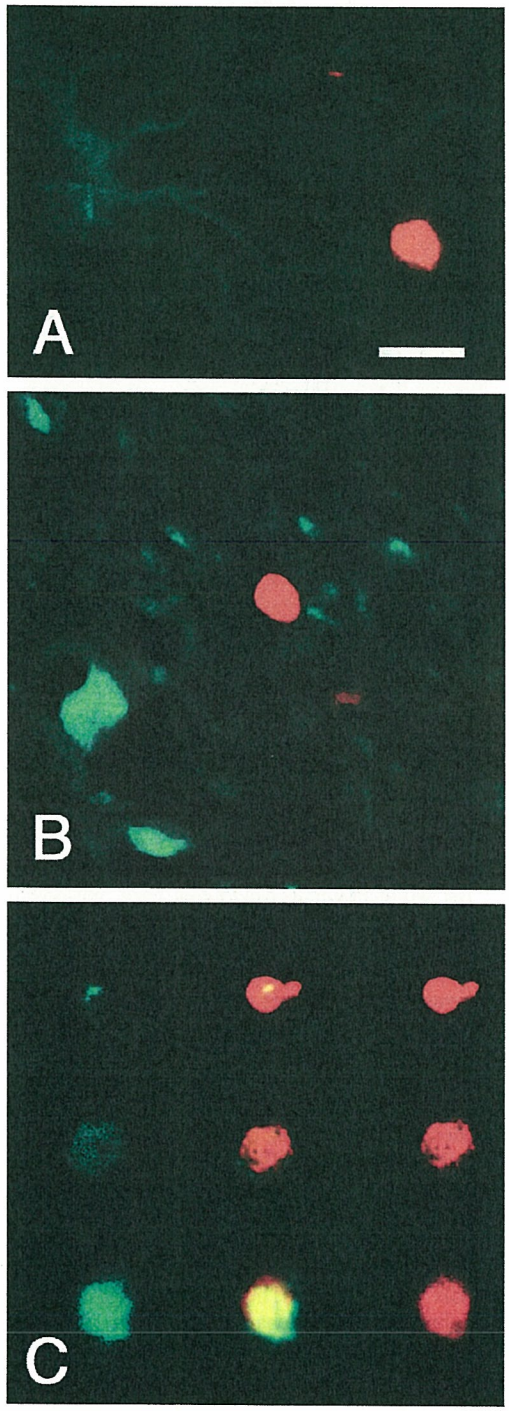

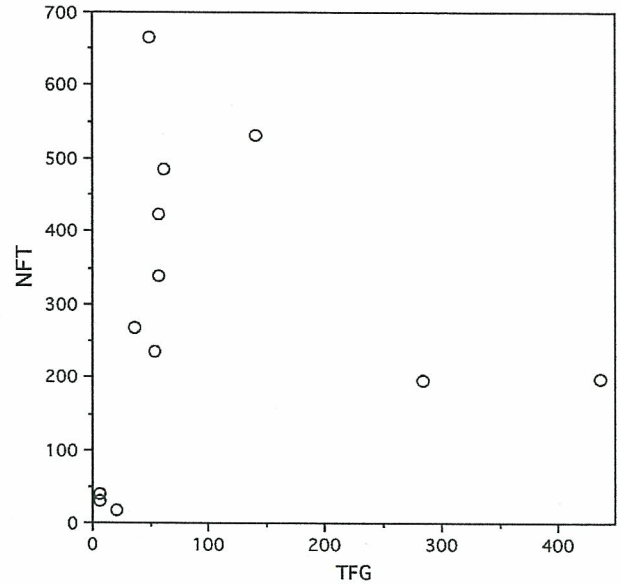

FIGURE 5. Relationship between the densities of neurofibrillary tangles (NFTs) and tau-positive fine granules (TFGs) in Guam parkinsonism–dementia complex (PDC). The number of TFGs was counted in a 100-μm^2 area of frontal white matter and the number of NFTs was counted in a 100-μm length of the frontal cortex. No significant relationship was found between the numbers of NFTs and TFGs in the frontal brains of patients with Guam PDC. However, it is safe to say that TFGs only seem to develop when the number of NFTs reaches a certain threshold level.

Furthermore, only a few of the Guamanian controls and Guamanian patients with ALS with many NFTs also exhibited TFGs. Globe-shaped and tau-positive inclusions like TFGs have never been described previously, although other tau-positive inclusions have been reported. Immunoelectron microscope observations revealed that putative TFGs are tau-positive structures that take the shape of granules with a diameter of 20 to 30 nm (including the DAB coating). The PDC white matter stained with Klüver-Barrera and Bodian did not mark a significant change in the stainability even in cases with many TFGs, despite atrophy of the white matter TFGs might relate to this peculiar degeneration of the PDC white matter. We became interested in whether the presence of TFGs had a connection to the atrophy of white matter in the PDC brain.

Immunofluorescence double labeling of TFGs, observed with the aid of confocal scanning microscopy, revealed no

FIGURE 4. Confocal scanning microscope observations made with the aid of immunofluorescence double labeling. GFAP ([A], green) and phosphorylated neurofilament ([B], green; SMI 31) were not localized on tau-positive fine granules (TFGs) (red; AT8). (C) Ubiquitin (green; left) was localized with tau (AT8, red; right) on TFGs in various distribution patterns (merged images) from only a small part (center) of the TFG to staining throughout most of the TFG (lower stand). Scale bars: 5 μm.

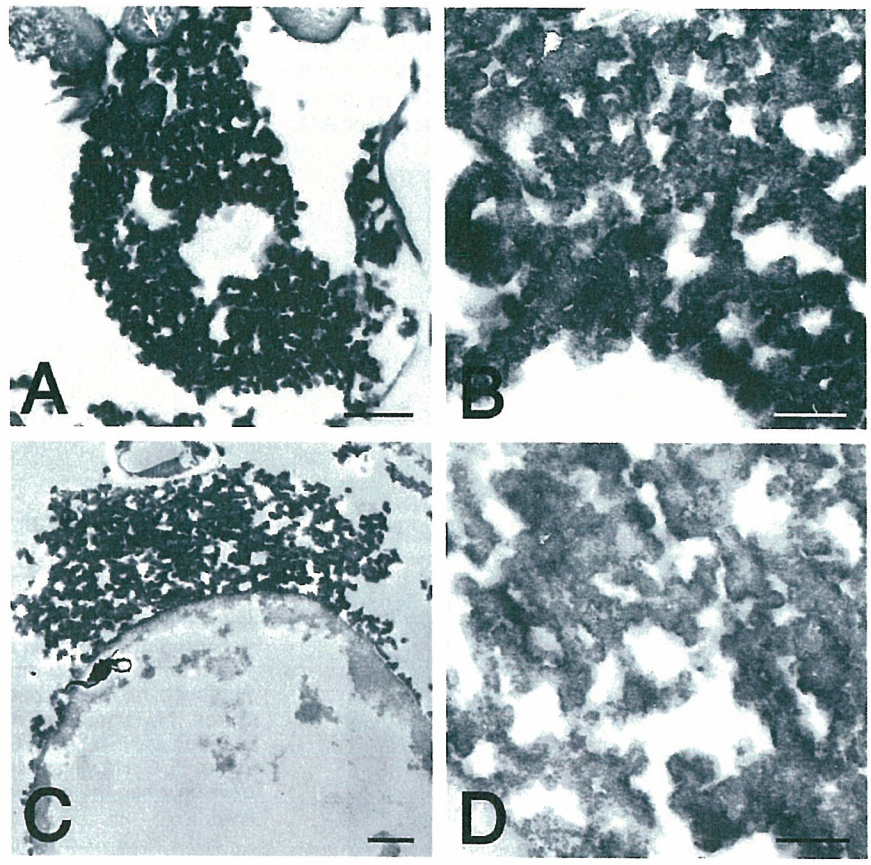

FIGURE 6. Immunoelectron microscope analysis of tau-positive fine granules (TFGs). **(A)** AT8-positive TFGs had some contact with the myelin outer loop (arrow) and no TFGs were observed either within the myelin sheath itself or the axons. **(B)** Examination of high-power views revealed that TFGs are permeated by round structures that are 20 to 30 nm in diameter (including the DAB substrate). **(C, D)** Similar structures were observed near the nucleus of the glial cells that were thought to be oligodendroglia. Scale bars = **(A, C)** 300 nm; **(B, D)** 100 nm.

colocalization of GFAP and tau staining or of phosphorylated neurofilament and tau staining on these structures. Therefore, it is unlikely that TFGs originate from either astrocytes or axons. TFGs that were closely associated with the outer layer of the myelin sheath were occasionally bordered by the nucleus of what appeared to be oligodendroglia. It is thus likely that TFGs are derived from oligodendroglia.

Many abnormal tau-positive structures in oligodendroglial cells such as ATs and coiled bodies have been observed in human brains (31–34). These structures are invariably observed in brains with CBD and PSP, but are not specific to neurodegenerative disorders. There are no previous reports of disease-specific oligodendroglial tau-positive inclusions that are a pathologic marker for tauopathies. Numerous tau-positive structures have been observed in the white matter of CBD brains (35, 36), and it is difficult to state categorically that no TFGs exist in the CBD white matter. However, none were observed in the CBD brains that were examined in the present study. TFGs bear a striking resemblance to argyrophilic grains morphologically, but the distribution of argyrophilic grains is quite different from that of TFGs. In AGD, argyrophilic grains are observed in cerebral cortex, amygdala, hypothalamus, and claustrum, but the deep white matter of frontotemporal lobes does not contain argyrophilic grains (37). In this study, tiny thread-like structures were also observed in the vicinity of TFGs in PDC. However, these structures were also detected in brains with CBD, PSP, Pick disease, AGD, and AD.

These structures are therefore not specific to any one tauopathy. Recently, Powers et al reported a case with novel leukoencephalopathy associated with tau deposits primarily in the glia of the white matter (38). In this case, tau-positive structures similar to TFGs were observed mainly in the frontal white matter. However, ultrastructurally, these tau deposits look completely different from TFGs, appearing in the form of straight filaments with a diameter of approximately 10 nm.

In Guam, cases of PDC with many NFTs also had many TFGs in the white matter, whereas in those cases with relatively small numbers of NFTs, TFGs were observed only rarely. Similarly, controls and cases of ALS with few NFTs had a small number of TFGs. Thus, it appears that TFGs only develop when the number of NFTs reaches a certain threshold. However, on further investigation, we found no significant lineal correlation between the presence of TFGs and the number of NFTs and granular hazy astrocytes (6). In addition, NFTs are known to be involved in fibril formation, but we found no fibrils in the TFGs. These results suggest that in Guam PDC brains, the mechanisms of tau deposition underlying the formation of NFTs and TFGs are different.

The presence of TFGs in patients with Guam PDC and Guam ALS does not prove that Guam ALS is a different

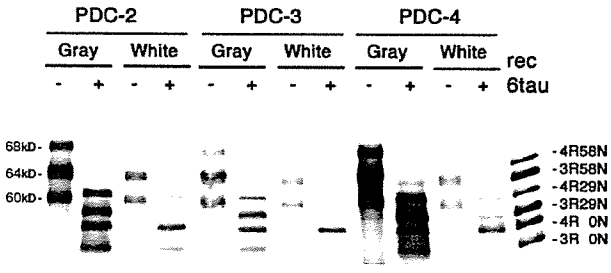

FIGURE 7. Western blot analysis of sarkosyl-insoluble tau from the frontal lobe of parkinsonism–dementia complex of Guam cases stained with the phosphorylation-independent anti-tau antibody, HT-7. HT-7 immunoblotting revealed the presence of 2 major bands of relative molecular mass 60 and 64 kDa, and one minor band of 68 kDa. After dephosphorylation, these bands appeared as one major band corresponding to a 4-repeat tau isoform with zero amino acid inserts (4R0N), 3 minor bands corresponding to a 4-repeat tau isoform with 29 amino acids inserts (4R29N), a 3-repeat tau isoform with zero amino acid inserts (3R0N), and a 3-repeat tau isoform with 29 amino acid inserts (3R29N). Recombinant tau isoforms were confined to the right side. Gray = gray matter; white = white matter.

disease from classic ALS or that Guam PDC and Guam ALS represent a single disease entity. The number of TFGs in many patients with Guam ALS was similar to that in nonPDC, nonALS control subjects. This finding indicates that TFGs are typical features of the general Guamanian population, as is the case with NFTs and granular hazy astrocytes. Moreover, our biochemical analysis revealed that the tau in the white matter of Guam PDC brains is composed of 4R tau. Some previous reports have shown that the tangles present in AD and PDC brains share the same profile when examined immunohistochemically with antihyperphosphorylated tau antibodies, and all 6 tau isoforms have been observed in tangle formation in Guamanian PDC as well as in AD brains (39, 40). A biochemical study of PDC brains in from individuals living on the Kii Peninsula also revealed that the dephosphorylated PHF tau protein is composed of all 6 isoforms (41). Until now, a regional biochemical analysis of tau proteins had not been carried out, and the present study represents the first biochemical analysis of the white matter of PDC brains (42–47). The results presented here show clearly that after dephosphorylation, the extracted insoluble tau is composed predominantly of the 4R tau isoforms, and that all 6 isoforms can be found in the frontal cortex (gray matter).

In recent years, it has been shown that the tau in sporadic Pick disease (48, 49) and in hereditary FTDP-17 (L266V) is composed of more than one tau isoform (3R and 4R tauopathies) (50). In the study presented here, it has been demonstrated that in Guamanian PDC, there are 2 distinct patterns of tau isoform composition; all 6 tau isoforms occur in the cerebral cortex and the 4R tau isoforms predominantly occur in the cerebral white matter. This is the first report of the existence of this combination of tau isoforms. Because the 4R tau predominant pattern was most obvious in cases in which TFGs were abundant in the white matter, these 4R tau isoforms are thought to reflect the biochemical characteristics of TFG. This raises the possibility that tau accumulates in those neurons expressing both 3R tau and 4R tau in the cerebral cortex and that tau builds up in those glial cells expressing 4R tau in the white matter. These glial cells exhibited tau isoform patterns such as 4R0N major, 4R29N, 3R0N, and 4R0N minor. Only one pattern of tau isoform was expressed in any one cell type, and the isoform of accumulated tau was dependent on which cells were involved in the lesions.

In a recent study, "tau-immunoreactive inclusions in glial cells in the white matter" resembling TFGs have been reported in cases with "primary progressive aphasia as the initial manifestation of corticobasal degeneration and unusual tauopathies" (51). Although these globular glial inclusions in the white matter are very similar to TFGs in Guamanian PDC, their size is reportedly larger than that of TFGs. In addition, the Western blotting analysis of total brain homogenates carried out in the present study showed 2 bands of relative molecular mass 68 and 64 kDa, in common with CBD but differing from Guam PDC white matter. It is hoped that these "tau-immunoreactive glial inclusions in the white matter" will be investigated further with the aid of immunoelectron microscopy.

In this study, TFGs were found exclusively in PDC brains and could therefore be a characteristic neuropathologic marker of this disease. The tau isoform in the gray matter (3R + 4R tau) was different from that in the white matter (4R tau) in PDC. This difference is thought to be a function of the cell type from which the tau originated. If this is the case, the question remains as to why particular tau isoforms prevail in the different cell types in any particular brain region and what mechanism underlies this process. The mechanism underlying disease-specific and tau-positive ultrastructural formations should be clarified in accordance with their particular tau isoform.

ACKNOWLEDGMENTS

The authors thank Dr. Hitoshi Takahashi, Department of Pathology, Brain Research Institute, Niigata University; and Ms. Emiko Kawakami, Department of Neuropathology, Tokyo Metropolitan Institute for Neuroscience, for their cooperation in this research.

REFERENCES

1. Spillantini MG, Murrell JR, Goedert M, et al. Mutation in the tau gene in familial multiple system tauopathy with presenile dementia. Proc Natl Acad Sci U S A 1998;95:7737–41
2. Spillantini MG, Goedert M. Tau protein pathology in neurodegenerative disease. Trends Neurosci 1998;21:428–33
3. Hirano A, Malamud N, Kurland LT. Parkinsonism–dementia complex, an endemic disease on the island of Guam. II. Pathological features. Brain 1961;84:662–79
4. Hof PR, Perl DP, Loerzel AJ, Morrison JH. Neurofibrillary tangle distribution in the cerebral cortex of parkinsonism–dementia cases from Guam: Differences with Alzheimer's disease. Brain Res 1991;564:306–13
5. Hof PR, Delacourte A, Bouras C. Distribution of cortical neurofibrillary tangles in progressive supranuclear palsy: A quantitative analysis of six cases. Acta Neuropathol (Berl) 1992;84:45–51
6. Oyanagi K, Makifuchi T, Ohtoh T, et al. Distinct pathological features of the Gallyas- and tau-positive glia in the parkinsonism–dementia complex and amyotrophic lateral sclerosis of Guam. J Neuropathol Exp Neurol 1997;56:308–16
7. Vermersch P, Sergeant N, Ruchoux MM, et al. Specific tau variants in the brains of patients with myotonic dystrophy. Neurology 1996;47:711–17

8. Oyanagi K, Wada M. Neuropathology of parkinsonism–dementia complex and amyotrophic lateral sclerosis of Guam: An update. J Neurol 1999; 246(suppl 2):II19–27
9. Oyanagi K, Makifuchi T, Ohtoh T, et al. Topographic investigation of brain atrophy in parkinsonism–dementia complex of Guam: A comparison with Alzheimer's disease and progressive supranuclear palsy. Neurodegeneration 1994;3:301–4
10. Oyanagi K, Makifuchi T, Ohtoh T, et al. The neostriatum and nucleus accumbens in parkinsonism-dementia complex of Guam: A pathological comparison with Alzheimer's disease and progressive supranuclear palsy. Acta Neuropathol (Berl) 1994;88:122–28
11. Oyanagi K, Makifuchi T, Ohtoh T, et al. Amyotrophic lateral sclerosis of Guam: The nature of the neuropathological findings. Acta Neuropathol (Berl) 1994;88:405–12
12. Oyanagi K, Tsuchiya K, Yamazaki M, Ikeda K. Substantia nigra in progressive supranuclear palsy, corticobasal degeneration, and parkinsonism–dementia complex of Guam: Specific pathological features. J Neuropathol Exp Neurol 2001;60:393–402
13. Wada M, Uchihara T, Nakamura A, Oyanagi K. Bunina bodies in amyotrophic lateral sclerosis on Guam: A histochemical, immunohistochemical and ultrastructural investigation. Acta Neuropathol (Berl) 1999;98:150–56
14. Oda T, Kogure T, Tominaga I, et al. An autopsy case of progressive supranuclear palsy with echolalia showing psychiatric symptoms at the beginning. J Clin Psychiatry 1994;36:1159–66
15. Tsuchiya K, Miyazaki H, Ikeda K, et al. Serial brain CT in corticobasal degeneration: Radiological and pathological correlation of two autopsy cases. J Neurol Sci 1997;152:23–29
16. Tsuchiya K, Uchihara T, Oda T, et al. Basal ganglia lesions in corticobasal degeneration differ from those in Pick's disease and progressive supranuclear palsy. A topographic neuropathological study of six autopsy cases. Neuropathology 1997;17:208–16
17. Tsuchiya K, Ikeda K, Uchihara T, et al. Distribution of cerebral cortical lesions in corticobasal degeneration: A clinicopathological study of five autopsy cases in Japan. Acta Neuropathol 1997;94:416–24
18. Tsuchiya K, Ikeda M, Hasegawa K, et al. Distribution of cerebral cortical lesions in Pick's disease with Pick bodies: A clinicopathological study of six autopsy cases showing unusual clinical presentations. Acta Neuropathol (Berl) 2001;102:553–71
19. Tsuchiya K, Ishizu H, Nakano I, et al. Distribution of basal ganglia lesions in generalized variant of Pick's disease: A clinicopathological study of four autopsy cases. Acta Neuropathol (Berl) 2001;102:441–48
20. Tsuchiya K, Ikeda K. Basal ganglia lesions in 'Pick complex': A topographic neuropathological study of 19 autopsy cases. Neuropathology 2002;22:323–36
21. Arai T, Ikeda K, Akiyama H, et al. Distinct isoforms of tau aggregated in neurons and glial cells in brains of patients with Pick's disease, corticobasal degeneration and progressive supranuclear palsy. Acta Neuropathol (Berl) 2001;101:167–73
22. Ikeda K, Akiyama H, Iritani S, et al. Corticobasal degeneration with primary progressive aphasia and accentuated cortical lesion in superior temporal gyrus: Case report and review. Acta Neuropathol (Berl) 1996;92:534–39
23. Arai Y, Yamazaki M, Mori O, et al. α-Synuclein-positive structures in cases with sporadic Alzheimer's disease: Morphology and its relationship to tau aggregation. Brain Res 2001;888:287–96
24. Yamazaki M, Nakano I, Imazu O, et al. Astrocytic straight tubules in the brain of a patient with Pick's disease. Acta Neuropathol (Berl) 1994;88:587–91
25. Yamazaki M, Nakano I, Imazu O, Terashi A. Paired helical filaments and straight tubules in astrocytes: An electron microscopic study in dementia of the Alzheimer type. Acta Neuropathol (Berl) 1995;90:31–36
26. Saito Y, Nakahara K, Yamanouchi H, Murayama S. Severe involvement of ambient gyrus in dementia with grains. J Neuropathol Exp Neurol 2002;61:789–96
27. Ihara Y. Massive somatodendritic sprouting of cortical neurons in Alzheimer's disease. Brain Res 1988;459:138–44
28. Yamazaki M, Arai Y, Baba M, et al. Alpha-synuclein inclusions in amygdala in the brains of patients with the parkinsonism–dementia complex of Guam. J Neuropathol Exp Neurol 2000;59:585–91
29. Goedert M, Spillantini MG, Cairns NJ, Crowther RA. Tau proteins of Alzheimer paired helical filaments: Abnormal phosphorylation of all six brain isoforms. Neuron 1992;8:159–68
30. Umeda Y, Taniguchi S, Arima K, et al. Alterations in human tau transcripts correlate with those of neurofilament in sporadic tauopathies. Neurosci Lett 2004;359:151–54
31. Chin SS-M, Goldman JE. Glial inclusions in CNS degenerative diseases. J Neuropathol Exp Neurol 1996;55:499–508
32. Feany MB, Mattiace LA, Dickson DW. Neuropathologic overlap of progressive supranuclear palsy, Pick's disease and corticobasal degeneration. J Neuropathol Exp Neurol 1996;55:53–67
33. Komori T. Tau-positive glial inclusions in progressive supranuclear palsy, corticobasal degeneration and Pick's disease. Brain Pathol 1999;9:663–79
34. Ikeda K, Akiyama H, Arai T, Nishimura T. Glial tau pathology in neurodegenerative diseases: Their nature and comparison with neuronal tangles. Neurobiol Aging 1998;19:S85–91
35. Wakabayashi K, Oyanagi K, Makifuchi T, et al. Corticobasal degeneration: Etiopathological significance of the cytoskeletal alterations. Acta Neuropathol (Berl) 1994;87:545–53
36. Feany MB, Dickson DW. Widespread cytoskeletal pathology characterizes corticobasal degeneration. Am J Pathol 1995;146:1388–96
37. Tolnay M, Clavaguera F. Argyrophilic grain disease: A late-onset dementia with distinctive features among tauopathies. Neuropathology 2004;24:269–83
38. Powers JM, Byrne NP, Ito M, et al. A novel leukoencephalopathy associated with tau deposits primarily in white matter glia. Acta Neuropathol (Berl) 2003;106:181–87
39. Buee-Scherrer V, Buee L, Hof PR, Leveugle B, et al. Neurofibrillary degeneration in amyotrophic lateral sclerosis/parkinsonism–dementia complex of Guam. Immunochemical characterization of tau proteins. Am J Pathol 1995;146:924–32
40. Goedert M, Spillantini MG, Cairns NJ, Crowther RA. Tau protein of Alzheimer paired helical filaments: Abnormal phosphorylation of all six brain isoforms. Neuron 1992;8:159–68
41. Kuzuhara S, Kokubo Y, Sasaki R, et al. Familial amyotrophic lateral sclerosis and parkinsonism–dementia complex of the Kii Peninsula of Japan: Clinical and neuropathological study and tau analysis. Ann Neurol 2001;49:501–11
42. Mawal-Dewan M, Schmidt ML, Balin B, et al. Identification of phosphorylation sites in PHF-TAU from patients with Guam amyotrophic lateral sclerosis/parkinsonism–dementia complex. J Neuropathol Exp Neurol 1996;55:1051–59
43. Trojanowski JQ, Ishihara T, Higuchi M, et al. Amyotrophic lateral sclerosis/parkinsonism dementia complex: Transgenic mice provide insights into mechanisms underlying a common tauopathy in an ethnic minority on Guam. Exp Neurol 2002;176:1–11
44. Forman MS, Schmidt ML, Kasturi S, et al. Tau and alpha-synuclein pathology in amygdala of parkinsonism–dementia complex patients of Guam. Am J Pathol 2002;160:1725–31
45. Schmidt ML, Zhukareva V, Perl DP, et al. Spinal cord neurofibrillary pathology in Alzheimer disease and Guam parkinsonism–dementia complex. J Neuropathol Exp Neurol 2001;60:1075–86
46. Schmidt ML, Garruto R, Chen J, et al. Tau epitopes in spinal cord neurofibrillary lesions in Chamorros of Guam. Neuroreport 2000;11:3427–30
47. Pérez-Tur J, Buée L, Morris HR, et al. Neurodegenerative diseases of Guam: Analysis of *TAU*. Neurology 1999;53:411–13
48. Zhukareva V, Mann D, Pickering-Brown S, et al. Sporadic Pick's disease: A tauopathy characterized by a spectrum of pathological tau isoforms in gray and white matter. Ann Neurol 2002;51:730–39
49. Zhukareva V, Shah K, Uryu K, et al. Biochemical analysis of tau proteins in argyrophilic grain disease, Alzheimer's disease, and Pick's disease: A comparative study. Am J Pathol 2002;161:1135–41
50. Hogg M, Grujic ZM, Baker M, et al. The L266V tau mutation is associated with frontotemporal dementia and Pick-like 3R and 4R tauopathy. Acta Neuropathol (Berl) 2003;106:323–36
51. Ferrer I, Hernandez I, Boada M, et al. Primary progressive aphasia as the initial manifestation of corticobasal degeneration and unusual tauopathies. Acta Neuropathol (Berl) 2003;106:419–35

Available online at www.sciencedirect.com
SCIENCE DIRECT®
Neuroscience Letters 380 (2005) 284–288
Neuroscience Letters
www.elsevier.com/locate/neulet

Oxidized galectin-1 advances the functional recovery after peripheral nerve injury

Toshihiko Kadoya [a,*], Kiyomitsu Oyanagi [b], Emiko Kawakami [b], Mitsuhiro Hasegawa [c], Yoshimasa Inagaki [d], Yoshiaki Sohma [d], Hidenori Horie [e]

[a] *CMC R&D Laboratories, Pharmaceutical Division, Kirin Brewery Co. Ltd., Hagiwara, Takasaki, Gunma 370-0013, Japan*
[b] *Department of Neuropathology, Tokyo Metropolitan Institute for Neuroscience, Musashidai, Fuchu, Tokyo 183-8526, Japan*
[c] *Department of Neurosurgery, Division of Neuroscience, Graduate School of Medical Science, Kanazawa University, Takara-machi, Kanazawa, Ishikawa 920-0934, Japan*
[d] *Pharmaceutical Research Laboratory, Pharmaceutical Division, Kirin Brewery Co. Ltd, Miyahara, Takasaki, Gunma 370-1295, Japan*
[e] *Advanced Research Center for Biological Science, Waseda University, Higashi-Fushimi, Nishi-Tokyo, Tokyo 202-0021, Japan*

Received 12 October 2004; received in revised form 28 December 2004; accepted 19 January 2005

Abstract

Oxidized galectin-1 has been shown to promote axonal regeneration from transected-nerve sites in an in vitro dorsal root ganglion (DRG) explant model as well as in in vivo peripheral nerve axotomy models. The present study provides evidence that oxidized galectin-1 advances the restoration of nerve function after peripheral nerve injury. The sciatic nerve of adult rats was transected and the distal nerve was frozen after being sutured into a proximal site with four epineurial stitches. An osmotic pump delivered oxidized galectin-1 peripherally to the surgical site. Functional recovery was assessed by measurement of the degree of toe spread of the hind paw for 3 months after the sciatic nerve lesion. The recovery curves of toe spread in the test group showed a statistically significant improvement of functional recovery after day 21 by the application of oxidized recombinant human galectin-1 (rhGAL-1/Ox) compared to the control group. This functional recovery was supported by histological analysis performed by light microscopic examination. The regenerating myelinated fibers at the site 21 mm distal to the nerve-transected site were quantitatively examined at 100 days after the operation. The frequency distribution of myelinated fiber diameters showed that exogenous rhGAL-1/Ox increased the number and diameter of regenerating myelinated fibers; the number of medium-sized (6–11 μm in diameter) fibers increased significantly ($P < 0.05$). These results indicate that oxidized galectin-1 promotes the restoration of nerve function after peripheral nerve injury. Thus, rhGAL-1/Ox may be a factor for functional restoration of injured peripheral nerves.

Keywords: Oxidized galectin-1; Axonal regeneration; Sciatic nerve injury; Remyelination; Myelinated fiber; Functional recovery; Toe spread

Initiation of neural restoration after axotomy has been thought to be regulated by neurotrophic factors [1,17], however, it remains unclear what signal prompts the axons to send out new processes in response to nerve injuries [1]. Recently, we discovered that oxidized galectin-1 promotes initial axonal growth after axotomy in peripheral nerves [6,7,10]. Galectin-1 is a member of a family of β-galactoside-binding lectins and is intensely expressed in dorsal root ganglion (DRG) neurons, spinal cord motoneurons and Schwann cells in normal sciatic nerves of adult rodents [3,6,9,16]. Galectin-1 contains six cysteine residues and exhibits lectin activity in its reduced form [11,15]. However, our structural–activity relationship study revealed that galectin-1 promotes axonal regeneration only in its oxidized form, which contains three intramolecular disulfide bonds [10]. Therefore, it is necessary to distinguish between

Abbreviations: rhGAL-1, recombinant human galectin-1; rhGAL-1/Ox, oxidized recombinant human galectin-1; PBS, phosphate-buffered saline; DRG, dorsal root ganglion

* Corresponding author. Tel.: +81 27 353 7381; fax: +81 27 353 7400.
E-mail address: tkadoya@kirin.co.jp (T. Kadoya).

0304-3940/$ – see front matter © 2005 Elsevier Ireland Ltd. All rights reserved.
doi:10.1016/j.neulet.2005.01.054

oxidized galectin-1, which promotes axonal regeneration, and galectin-1, which shows lectin activity.

Using in vivo peripheral nerve regeneration models, we have demonstrated that the application of oxidized recombinant human galectin-1 (rhGAL-1/Ox) to the injured region promotes axonal growth [6]. Conversely, treatment with a functional blocking galectin-1 antibody strongly inhibits the restoration. These experiments show that oxidized galectin-1 is an essential factor for initiating axonal regeneration in injured peripheral nerves.

In the present study, we examined whether or not local administration of exogenous rhGAL-1/Ox advances the restoration of nerve function using a rat injured sciatic nerve model. The degree of toe spread [4] was measured for 3 months after the sciatic nerve lesion in order to assess functional recovery. Histological and quantitative studies [14] were also conducted after the functional assessment to evaluate the regeneration of myelinated fibers.

rhGAL-1/Ox was prepared as described previously [6,10]. Briefly, *Escherichia coli* expressed rhGAL-1 was purified by DEAE-HPLC and rhGAL-1 was oxidized by the air oxidation method using $CuSO_4$ as a catalyst. rhGAL-1/Ox was purified by reversed phase HPLC. A total of 36 adult male Sprague–Dawley rats (10 weeks) were used. The animals were randomly assigned to one of three groups of 12 animals each. In accordance with the guidelines of our institutional Animal Research Committee, we placed the animals two to a gage with a 12-h light:12-h dark cycle, and rat chow and water were available ad libitum.

In a previous study, we have shown that oxidized galectin-1 promotes axonal regeneration together as well as the Schwann cell migration into the acellular nerve or a grafted silicone tube filled with collagen gel [6]. In order to reproduce the appropriate acellular nerve conditions, we introduced a cut and freeze-killed sciatic nerve model. The operation was carried out according to the method previously described [13], with some modification. Briefly, the animals were anesthetized, to avoid unnecessary pain, with intraperitoneal sodium pentobarbital (60 mg/kg). The left sciatic nerve was exposed and transected at the mid-thigh level with microscissors. The distal stump was sutured into the proximal stump with four epineurial stitches of 8–0 Nylon, then 7 mm of distal nerve section was frozen for 10 s with forceps that had been chilled in liquid nitrogen. An osmotic pump (Alza Corp., 2 ml reservoir) was used to deliver test solutions peripherally, either rhGAL-1/Ox or PBS for control. The solutions were delivered at 2.5 μl/h from the polyethylene tube connected to the osmotic pump, which was implanted subcutaneously on the back, for a period of 4 weeks. Rats were divided into three groups of 12 rats each: a control group which was treated with phosphate buffered saline (PBS), and two test groups, one of which received 5 μg/ml of rhGAL-1/Ox solution applied to the surgical site, and one of which received 100 μg/ml of rhGAL-1/Ox solution. These concentrations of rhGAL-1/Ox solution were chosen because 5 μg/ml of rhGAL-1/Ox was found to be effective in a mouse model in our previous studies [3,6], and because a higher dose would be expected to advance functional recovery. No rats showed any toxic effects in reaction to the administration of rhGAL-1/Ox.

Functional recovery was evaluated by measuring the degree of toe spread [4], which is defined as the maximum distances between the first and fifth toes (toe spread) and between the second and fourth toes (intermediary toe spread) of the hind paw. Both toe spreads were measured at 1, 3, 7, 14, 21, 28, 35, 42, 49, 56, 63, 70, 77, and 84 days postoperatively with calipers at the tips of the toes by holding the rat's back from behind and pushing the paw slightly to the floor. The distance of the toe spread were not dependent on the pushing strength and reproducibility of the data was very good; note that the pressure exerted on the hind paw remains constant regardless of pushing strength because the rat's pelvis absorbs any extra pressure beyond that which produces the toe spread. All measurements were carried out at least three times, and the values were averaged ($n = 12$ for each group).

After the functional assessment, 14 rats (four in the PBS group, four in the 100 μg/ml rhGAL-1/Ox group, two in the 5 μg/ml rhGAL-1/Ox group and four in an unoperated group) were perfused through the heart and fixed with 2.5% glutaraldehyde, 1% paraformaldehyde in 0.1 M sodium cacodylate. The fixed sciatic nerve was dehydrated through a graded ethanol series and embedded in EPON 812. Cross sections (1 μm-thick) were cut 21 mm distal to the transection site, then stained with toluidine blue and examined under a light microscope. The quantitative analysis of regenerating myelinated axons was performed as described previously [14]. Briefly, photographs of three randomly chosen areas (16,870 μm2 each) of the cross sections were taken (×200 magnification). Enlarged prints (×2200 magnification) were made, and a digitizer was used to obtain the mean diameter of the myelinated fibers by averaging the longest and shortest diameters (the latter being perpendicular to the former). The data for the three areas were summed and converted to numerical values per total area of the cross section, and the frequency distribution of the myelinated axon diameters, in 1-μm increments, was determined. Statistical analysis of the experiments was performed using StatView for Macintosh (SAS Institute, Cary, NC). Significant differences between groups were determined by two-way ANOVA. Data are presented as the mean ± S.E.M. $P < 0.05$ between any two groups was considered significant according to the Bonferroni procedure.

Motor nerve conduction velocity (MNCV) was measured using 18 rats with the same operation mentioned above: 10 rats were received PBS and eight were received 100 μg/ml rhGAL-1/Ox. MNCV was measured on left sciatic nerve at day 84 after the operation using MEB-7102 instrument (Nihon Koden, Osaka, Japan). Measurements were performed under general anesthesia using halothane and the body temperature of the animals was kept constant at 37 °C. The comparisons between the groups for MNCV were performed using an unpaired t-test.

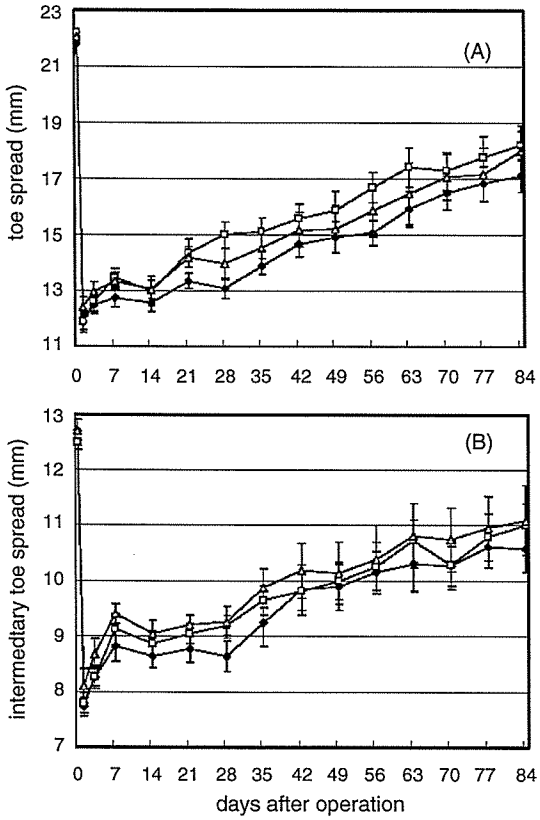

Fig. 1. Rates of functional recovery after sciatic nerve injury. Functional recovery was evaluated by the degree of toe spread (A) and intermediary toe spread (B) of the hind paw. (♦) PBS control group; (△) 100 μg/ml rhGAL-1/Ox group; (□) 5 μg/ml rhGAL-1/Ox group. Data are mean ± S.E.M. ($n = 12$).

At 12 weeks after the operation, the nerve repair sites and pump delivery systems were intact and there was no difference between the PBS group and the two rhGAL-1/Ox groups. Recovery curves drawn from the toe spread and intermediary toe spread data are shown in Fig. 1. Statistical analysis of the recovery curves in the early period until postoperative day 14 revealed no significant differences among the three groups. After postoperative day 21, however, the recovery curves of intermediary toe spread showed a significant difference between the PBS group and the 5 and 100 μg/ml rhGAL-1/Ox groups (P value <0.05 by analysis of variance, ANOVA). The recovery curves of toe spread after postoperative day 21 also showed significant differences between the PBS group and the two rhGAL-1/Ox groups (P value <0.05 by ANOVA), with a significantly improved rate of recovery in injured nerves supplemented by the delivery of exogenous rhGAL-1/Ox.

Histological analysis was performed by light microscopic examination after the functional assessment. The regenerating axons at 100 days after operation were observed at a site 21 mm distal to the nerve-transected site (Fig. 2), and the numbers of regenerating myelinated fibers were quantitatively examined (Fig. 3). The frequency distribution of myelinated fiber diameters showed that the number of

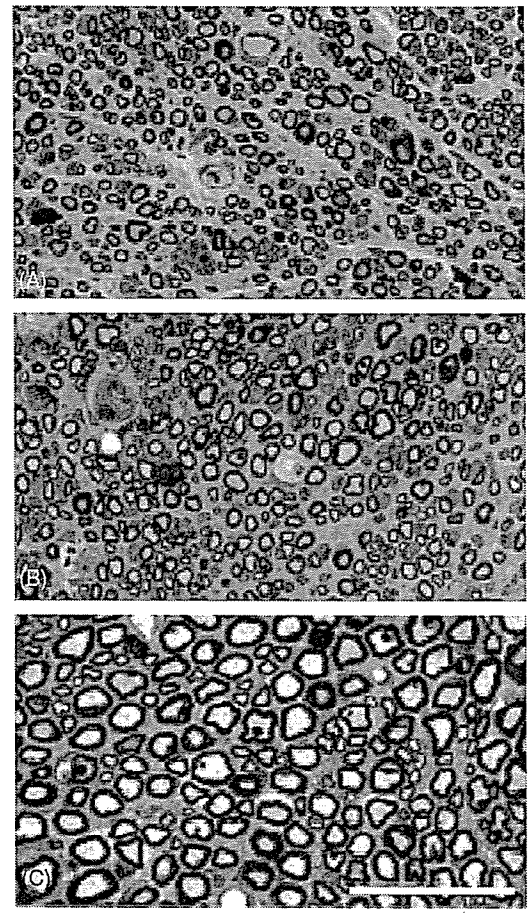

Fig. 2. Light micrographs of the sciatic nerves. At 100 days after operation, the cross sections at a site 21 mm distal to the nerve-transected site in the operated rat and the exact same position in the normal control rat were stained with toluidine blue. (A) PBS control; (B) rhGAL-1/Ox 100 μg/ml; and (C) unoperated control. Scale bar: 50 μm.

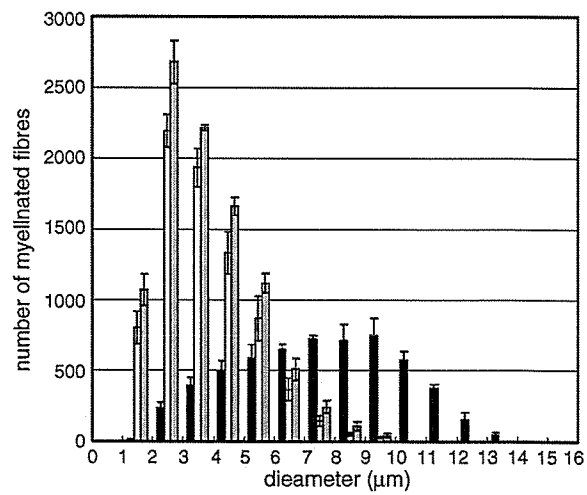

Fig. 3. Fiber-size distribution of the myelinated fibers in the cross sections at a site 21 mm distal to the nerve-transected site 100 days after operation. Unoperated group (closed bar), PBS control group (open bar), 100 μg/ml rhGAL-1/Ox group (striped bar). Data are means ± S.E.M. ($n = 4$).

Table 1
MNCV in the sciatic nerve at 84 days after the operation

PBS group ($n=10$)		100 μg/ml rhGAL-1/Ox ($n=8$)	
Animal number	MNCV (m/s)	Animal number	MNCV (m/s)
1	23.8	1	19.6
2	20.6	2	29.8
3	27.7	3	20.1
4	23.9	4	30.3
5	19.9	5	21.5
6	23.1	6	27.1
7	24.5	7	35.3
8	26.0	8	30.9
9	21.9		
10	23.6		

regenerating myelinated fibers was significantly higher in the 100 μg/ml rhGAL-1/Ox group than in the PBS control group (P values <0.05 by ANOVA), and the total number of regenerating myelinated fibers was approximately 6 and 26% higher in the 5 and 100 μg/ml groups, respectively, than in the PBS control group. The numbers of medium-sized myelinated fibers (6–11 μm in diameter) were especially increased in the rhGAL-1/Ox groups, averaging 983.4 ± 168.8 (100 μg/ml, $n=4$) and 846.8 ± 136.2 (5 μg/ml, $n=2$); on the other hand, in the PBS group, only 580.6 ± 128.4 ($n=4$) was the average.

MNCV was measured to confirm the recovery promoting effect of rhGAL-1/Ox. Table 1 shows the results of MNCV measurement at 84 postoperative days. MNCV in PBS treated group was 23.5 ± 0.7 ($n=10$), indicating that the operation was reproducible enough to perform the evaluation. Compared to the control group, the data in rhGAL-1/Ox treated group was divided into two groups; five of the 8 rats showing large MNCV (29.8, 30.3, 27.1, 35.3, and 30.9), and the other three rats showing small MNCV (19.6, 20.1, 21.5). The average of the small MNCV group (20.4 ± 0.6, $n=3$), which was seemed to be similar to that of the control group, was clearly different from that of the large MNCV group (30.7 ± 1.3, $n=5$). This division might be due to insufficient supply of the factor into the operated region. MNCV of the large MNCV group was specifically different from that of the control group (P value <0.005 by an unpaired t-test).

In our previous study [6], the acceleration of axonal regeneration by oxidized galectin-1 was shown by the application of rhGAL-1/Ox to in vivo injured peripheral nerve models. Recently, Fukaya et al. [3] investigated the effects of oxidized galectin-1 on the regeneration of rat spinal nerves using acellular autografts and allografts during the period of one to 2 weeks after the injury, with special attention to the relationship between axonal regeneration and Schwann cell migration. The administration of rhGAL-1/Ox was found to promote axonal regeneration from motoneurons as well as from DRG neurons; this was confirmed by a fluorogold tracer study [3]. Moreover, the migration of Schwann cells from both proximal and distal stumps was enhanced, and Schwann cell migration was found to precede axonal growth in the presence of exogenous rhGAL-1/Ox in the grafts. These results strongly suggest that oxidized galectin-1 is a key factor in the initial stages of axonal regeneration.

The present study provides evidence in favor of the idea that oxidized galectin-1 advances the restoration of nerve function after peripheral nerve injury. Functional recovery was evaluated by measuring the degree of toe spread because this examination is a simple and easily available method of evaluating the effects of given factors on functional recovery after sciatic nerve injury [2,4]. Fig. 1 shows that the rhGAL-1/Ox groups experienced functional recovery 1–2 weeks earlier than did the PBS group, which is consistent with data provided by studies on treatment with brain-derived neurotrophic factor (BDNF) or other trophic factors [5,12,13,18]. The functional recovery of both toe spread curves began to show a significant difference between the rhGAL-1/Ox groups and the PBS control group after postoperative day 21. Although further improvements were expected, the effect was limited to the initial advancement of recovery. This may be due to the method of application of rhGAL-1/Ox, which was supplied using a mini-osmotic pump. The operated site was quickly covered with connective tissues, preventing diffusion of rhGAL-1/Ox. A constant delivery system of rhGAL-1/Ox to the injured sites may make it possible to achieve further improvements in recovery.

The reconstruction of myelin in regenerating fibers is an important step for the restoration and functional recovery of injured nerves. Therefore, histological analysis was performed with special attention to the remyelination of the regenerating fibers after the functional assessment. Based on the fiber-size distribution of the myelinated fibers of unoperated axons (Fig. 3), it is clear that reconstruction of myelin in the operated groups is insufficient at 100 postoperative days. However, administration of rhGAL-1/Ox to the nerve injury site was found to increase both the number and the diameter of regenerating myelinated fibers, especially of medium-sized fibers. These histological and quantitative studies support the data obtained from our tests on functional recovery. The promotion of MNCV recovery by the treatment of rhGAL-1/Ox confirmed it.

The mechanism which controls how oxidized galectin-1 promotes peripheral nerve regeneration remains unclear. Recently, however, we have shown that macrophages are the target cells and that oxidized galectin-1 stimulates macrophages to secrete a factor that promotes axonal growth and Schwann cell migration [8]. This essential function of oxidized galectin-1 for peripheral nerve regeneration is thought to be specifically different from other known neurotrophic factors.

A factor that initiates the regeneration process is a candidate for enhancing nerve recovery, and oxidized galectin-1 seems to be one of the triggers of nerve regeneration [6–8,10]. The present study shows that administration of rhGAL-1/Ox to the sciatic nerve injury site improves functional recovery at a concentration (μg/ml order) at which no toxic phenomena were observed. Thus, rhGAL-1/Ox is potentially therapeutic for functional restoration after peripheral nerve injury.

Acknowledgements

This work was supported in part by grants from the Japanese Ministry of Education, Science, Sports and Culture (#14580735 to KO) and the Japanese Ministry of Health, Labor and Welfare (#H16-kokoro-017 of the Research on Psychiatric and Neurological Diseases and Mental Health to KO).

References

[1] S.C. Apfel, Clinical Application of Neurotrophic Factors, Lippincott-Raven Publishers, 1997.
[2] J.R. Bain, S.E. Mackinnon, D.A. Hunter, Functional evaluation of complete sciatic, peroneal, and posterior tibial nerve lesions in the rat, Plast. Reconstr. Surg. 83 (1989) 129–136.
[3] K. Fukaya, M. Hasegawa, T. Mashitani, T. Kadoya, H. Horie, Y. Hayashi, H. Fujisawa, O. Tachibana, S. Kida, J. Yamashita, Oxidized galectin-1 stimulates the migration of Schwann cells from both proximal and distal stumps of transected nerves and promotes axonal regeneration after peripheral nerve injury, J. Neuropathol. Exp. Neurol. 62 (2003) 162–172.
[4] K. Hasegawa, A new method of measuring functional recovery after crushing the peripheral nerves in unaneathetized and unrestrained rats, Experientia 34 (1978) 272–273.
[5] P.-R. Ho, G.M. Coan, E.T. Cheng, C. Niell, D.M. Tarn, H. Zhou, D. Sierra, D.J. Terris, Repair with collagen tubules linked with brain-derived neurotrophic factor and ciliary neurotrophic factor in a rat sciatic nerve injury model, Arch. Otolaryngol. Head Neck Surg. 124 (1998) 761–766.
[6] H. Horie, Y. Inagaki, Y. Sohma, R. Nozawa, K. Okawa, M. Hasegawa, N. Muramatsu, H. Kawano, M. Horie, H. Koyama, I. Sakai, K. Takeshita, Y. Kowada, M. Takano, T. Kadoya, Galectin-1 regulates initial axonal growth in peripheral nerves after axotomy, J. Neurosci. 19 (1999) 9964–9974.
[7] H. Horie, T. Kadoya, Identification of oxidized galectin-1 as an initial repair regulatory factor after axotomy in peripheral nerve, Neurosci. Res. 38 (2000) 131–137.
[8] H. Horie, T. Kadoya, N. Hikawa, K. Sango, H. Inoue, Y. Inagaki, K. Takeshita, R. Asawa, T. Hiroi, M. Sato, T. Yoshioka, Y. Ishikawa, Oxidized galectin-1 stimulates macrophages to promote axonal regeneration in peripheral nerves after axotomy, J. Neurosci. 24 (2004) 1873–1880.
[9] M.A. Hynes, M. Gitt, S.H. Barondes, T.M. Jessell, L.B. Buck, Selective expression of an endogenous lactose-binding lectin gene in subsets of central and peripheral neurons, J. Neurosci. 10 (1990) 1004–1013.
[10] Y. Inagaki, Y. Sohma, H. Horie, R. Nozawa, T. Kadoya, Oxidized galectin-1 promotes axonal regeneration in peripheral nerves but does not possess lectin properties, Eur. J. Biochem. 267 (2000) 2955–2964.
[11] K. Kasai, J. Hirabayashi, Galectins: a family of animal lectins that decipher glycocodes, J. Biochem. 119 (1996) 1–8.
[12] S.L. Lewin, D.S. Utley, E.T. Cheng, A.N. Verity, D.J. Terris, Simultaneous treatment with BDNF and CNTF after peripheral nerve transection and repair enhances rate of functional recovery compared with BDNF alone, Laryngoscope 107 (1997) 992–999.
[13] J.P. Newman, A.N. Verity, S. Hawatmeh, W.E. Fee, D.J. Terris, Ciliary neurotrophic factor enhances peripheral nerve regeneration, Arch. Otolaryngol. Head Neck Surg. 122 (1996) 399–403.
[14] K. Oyanagi, E. Kawakami, T. Morita, H. Takahashi, Pursuit of the origin of the large myelinated fibers of the anterolateral funiculus in the spinal cord in humans in relation to the pathomechanism in amyotrophic lateral sclerosis, Acta Neuropathol. 98 (1999) 635–640.
[15] N.L. Perillo, M.E. Marcus, L.G. Baum, Galectins: versatile modulators of cell adhesion, cell proliferlation, and cell death, J. Mol. Med. 76 (1998) 402–412.
[16] L.J. Regan, J. Dodd, S.H. Barondes, T.M. Jessell, Selective expression of endogenous lactose-binding lectins and lactoseries glycoconjugates in subsets of rat sensory neurons, Proc. Natl. Acad. Sci. U.S.A. 83 (1986) 2248–2252.
[17] G. Terenghi, Peripheral nerve regeneration and neurotrophic factors, J. Anat. 194 (1999) 1–14.
[18] D.S. Utley, S.L. Lewin, E.T. Cheng, A.N. Verity, D. Sierra, Brain-derived neurotrophic factor and collagen tubulization enhance functional recovery after peripheral nerve transection and repair, Arch. Otolaryngol. Head Neck Surg. 122 (1996) 407–413.

Acta Neuropathol (2005) 109: 457–466
DOI 10.1007/s00401-004-0971-7

REGULAR PAPER

Yorito Anamizu · Hiroshi Kawaguchi · Atsushi Seichi
Shinji Yamaguchi · Emiko Kawakami · Naotoshi Kanda
Shiro Matsubara · Makoto Kuro-o · Yoichi Nabeshima
Kozo Nakamura · Kiyomitsu Oyanagi

Klotho insufficiency causes decrease of ribosomal RNA gene transcription activity, cytoplasmic RNA and rough ER in the spinal anterior horn cells

Received: 8 September 2004 / Revised: 29 November 2004 / Accepted: 29 November 2004 / Published online: 16 April 2005

Abstract The *klotho* gene was identified in 1997 as the gene whose severe insufficiency (*kl/kl*) causes a syndrome resembling human aging, such as osteoporosis, arteriosclerosis, gonadal atrophy, emphysema, and short life span in a mouse strain. Regarding the gait disturbance reported in *kl/kl* mice, the present study examined the spinal cord of *kl/kl* mice, and revealed decreases in the number of large anterior horn cells (AHCs), the amount of cytoplasmic RNA, the number of ribosomes and rough endoplasmic reticulum (rER), and the activity of ribosomal (r) RNA gene transcription without significant loss of the total number of neurons in the ventral gray matter. Increased immunostaining of phosphorylated neurofilament in the AHCs and of glial fibrillary acidic protein in reactive astrocytes in the anterior horn of *kl/kl* mice were also observed. On the other hand, the posterior horn was quite well preserved. The results suggest that the *kl/kl* insufficiency causes atrophy and dysfunction of the spinal AHCs through decreased activity of rRNA gene transcription, which may reduce the amount of cytoplasmic RNA and the number of ribosomes and rER. These findings resemble those found in the spinal cord of patients with classic amyotrophic lateral sclerosis (ALS). The results show that *klotho* gene insufficiency causes dysfunction of the protein synthesizing system in the AHCs, and might indicate the *klotho* gene is involved in the pathological mechanism of classic ALS. The *kl/kl* is a new animal model of AHC degeneration, and may provide clues to understanding the etiology of classic ALS.

Keywords Anterior horn cell · Cytoplasmic RNA · Klotho · Ribosomal RNA gene · Transcription activity

Y. Anamizu · E. Kawakami · K. Oyanagi (✉)
Department of Neuropathology,
Tokyo Metropolitan Institute for Neuroscience,
2-6 Musashidai, Fuchu, 183-8526 Tokyo, Japan
E-mail: k123ysm@tmin.ac.jp
Tel.: +81-42-3253881 ext 4711
Fax: +81-42-3218678

Y. Anamizu · H. Kawaguchi · A. Seichi · K. Nakamura
Department of Orthopedic Surgery,
Graduate School of Medicine,
University of Tokyo, Tokyo, Japan

S. Yamaguchi
Department of Biochemistry,
Molecular Biology and Cell Biology, Northwestern University,
Evanston, Illinois, USA

N. Kanda
Department of Anatomy,
Graduate School of Veterinary Medicine,
Tokyo University of Agriculture and Technology,
Tokyo, Japan

S. Matsubara
Department of Neurology,
Tokyo Metropolitan Neurological Hospital,
Fuchu, Tokyo, Japan

M. Kuro-o
Department of Pathology,
University of Texas Southwestern Medical Center,
Dallas, Texas, USA

Y. Nabeshima
Department of Tumor Biology,
Graduate School of Medicine, Kyoto University,
Kyoto, Japan

Introduction

Mouse lines exhibiting symptoms of early-onset senescence have been established using insertion mutations; it has been shown that the absence of a single gene produces a variety of aging symptoms. The *klotho* gene has been identified as the causal gene at 5G3 in mice and 13q12 in humans [27]. Homozygotes with the *klotho* gene mutation (*kl/kl*) are reported to demonstrate phenotypes highly similar to human aging, including osteoporosis, calcification of articular cartilage and soft tissue, arteriosclerosis, decreased activity, emphysema,

and gonadal, thymic, and dermal atrophy. The life span is reported to be 8–9 weeks on average. The *kl/kl* mice are senescence-accelerated mice satisfying 7 among 21 of the pathophysiological and cellular criteria of aging [27]. An association between the allele of the functional variant of the *klotho* gene and occult coronary artery disease has been reported [3].

In addition to the above-mentioned symptoms, *kl/kl* mice exhibit an abnormal gait. Reduction in the number of cerebellar Purkinje cells [27] may be a factor relating to the gait disturbance, but the spinal cord has not been examined genetically or histologically. To date, there have been no reports on the expression of the *klotho* gene in the spinal cord. An age-related reduction of the number of small neurons in the anterior horn has been reported in humans [25, 26, 40], and it was thus important to examine whether or not similar changes occur in *kl/kl* mice. The purpose of the present study was to clarify the genetic, histological, quantitative and ultrastructural peculiarities in the spinal cord in *kl/kl* mice, and compare those with the findings in the human spinal cord in aging. We have found some degenerative changes, similar to those reported in the human anterior horn cells (AHCs) with neurodegenerative diseases including classic amyotrophic lateral sclerosis (ALS), in this senescence model mouse.

Materials and methods

Animals

All animals were bred and kept in a breeder (Clea-Japan Corp., Tokyo, Japan) until just before the sacrifice. At sacrifice, adequate measures were taken to minimize pain and discomfort to the animals, according to the "Guidelines for Experiments of the Tokyo Metropolitan Institute for Neuroscience". All animal experiments conformed to the United States Public Health Service's Policy on Human Care and Use of Laboratory Animals.

The genetic background of the original *klotho* mice was a mixture of C57BL/6J and C3H/J species. We used 21 male *kl/kl* mice and 19 male wild-type (WT) mice at the age of 7 weeks, the period assumed to be that just before death. Genotypes of the sacrificed mice were determined by Southern blot analyses using their tails and probes to detect the inserted plasmid located adjacent to the *klotho* gene locus. The body and brain weights were measured at the time of sacrifice (Table 1).

Table 1 The body and brain weight of *kl/kl* and WT mice at the age of 7 weeks. Values represent mean ± SD (*kl/kl* homozygotes with the *klotho* mutation, *WT* wild-type)

	Body weight (g)	Brain weight (g)
kl/kl (male, $n=17$)	7.6 ± 1.1*	0.37 ± 0.02*
WT (male, $n=17$)	24.4 ± 1.58	0.47 ± 0.03

*$P < 0.0001$

Animals were deeply anesthetized with ether before the processing. For reverse transcription (RT)-PCR, the cervical spinal cords from *kl/kl* and WT mice ($n=2$, respectively) were taken up in lysis buffer for the isolation of total RNA (RNeasy kit; Qiagen, Chatsworth, CA). Fifteen *kl/kl* and 13 WT male mice were transcardially perfused with 4% paraformaldehyde (PFA) in 0.1 M phosphate buffer (PB) (pH 7.3) for paraffin embedding. Four *kl/kl* and 4 WT mice were transcardially perfused with 2.5% glutaraldehyde (GA) and 1% PFA in 0.1 M cacodylate buffer (CB) (pH 7.3) for Epon embedding.

RT-PCR procedure of the spinal cord

RNA (0.3–1 μg) was dissolved in 30 μl H_2O, and the following was added: 2.5 μl 1 M TRIS (pH 7.4), 20 μl 25 mM $MgCl_2$, 2 μl RNase-free DNase (10 U/μl; Roche Molecular Biochemicals, Mannheim, Germany), and 0.5 μl RNasin (40 U/μl; Promega, Madison, WI). The mixture was incubated for 20 min at 37°C and subsequently divided into two parts. In one part, RNA was reverse-transcribed using oligo(dT) primers (Life Technologies, Rockville, MD) and Moloney murine leukemia virus reverse transcriptase (Superscript II; Life Technologies) at 45°C for 1 h. The other part was incubated in the same mixture without the enzyme and was later used as a control for DNA contamination in the PCR. The cDNA was purified (PCR purification kit; Qiagen) and used as a template for PCR in a 60-μl reaction volume containing 1× PCR buffer containing 1.5 mM $MgCl_2$ (Perkin-Elmer, Foster City, CA), 0.2 mM dNTPs, and 0.1 μM of each primer. Specific oligonucleotide primers (Life Technologies) for PCR were designed to amplify rat (GenBank accession no. AB005141) *klotho* mRNA (forward 5'-AGATGTGGCCAGCGATAGTTA-3'; reverse 5'-ACTTGACCTGACCACCGAAGT-3') [29]. A "hot start" was performed manually by adding 1.5 U AmpliTaq (Perkin-Elmer) after an initial incubation of 5 min at 95°C in a thermocycler (Perkin-Elmer, 9700). For each experiment the housekeeping gene glyceraldehyde-3-phosphate dehydrogenase (GAPDH) was amplified with 20 and 22 cycles to normalize the cDNA content of the samples. Equal cDNA amounts were subsequently used for the amplification of *klotho* gene. Amplification was performed for 20–40 cycles (94°C for 30 s, 50°C for 10 s, and 72°C for 90 s). The linear range of amplification was determined for each primer set. The amplicons were analyzed on a 1.5% agarose gel stained with ethidium bromide.

Histological and immunohistochemical examination

The 5th cervical and 4th lumbar segments were removed from the 4% PFA-fixed spinal cords under a dissecting microscope. Tissue blocks were dehydrated in ethanol

series, and embedded in paraffin. Serial transverse sections (6 μm thick) were made, and were subjected to hematoxylin-eosin, Klüver-Barrera (K-B) and pyronin Y preparation.

Sections, 6 μm thick, were also subjected to immunohistochemical staining using the avidin-biotin-peroxidase complex (ABC) method with a Vectastain ABC kit (Vector, Burlingame, CA). The primary antibodies used were rabbit anti-cow ubiquitin polyclonal antibody (dilution 1:150; Dakopatts, Glostrup, Denmark), SMI-31 monoclonal antibody (dilution 1:1,000; Sternberger Monoclonals, Baltimore, MD), and rabbit anti-glial fibrillary acidic protein (GFAP) polyclonal antibody (dilution 1:1,000; Dakopatts). Lectin histochemistry for microglia was performed using IB4 coupled to horseradish peroxidase (HRP) (dilution 1:100, Sigma, St. Louis, MO). Antigenicity was increased for ubiquitin immunostaining by pretreating the sections with 0.025% trypsin for 15 min at room temperature. Endogenous peroxidase activity was quenched by incubating the sections in 3% hydrogen peroxide in methanol and then blocked by incubating for 1 h with 3% normal goat or mouse serum in phosphate-buffered saline (PBS). The sections were incubated with the required primary antibody overnight at 4°C, then incubated with the secondary reagent containing biotinylated anti-rabbit or anti-mouse IgG (diluted 1:200) for 2 h, and finally with the ABC solution for 1 h. The sections were subjected to the peroxidase reaction using freshly prepared 0.02% 3,3'-diaminobenzidine-tetrahydrochloride and 0.005% hydrogen peroxide in 0.05 M TRIS-HCl buffer pH 7.6 for 10 min at room temperature. As antibody controls, the primary antisera were either omitted or replaced with normal rabbit or mouse serum. Several specimens of neural and non-neural tissue from the patients served as positive or negative tissue controls.

Quantitative examination of the neurons in the ventral spinal gray matter

The number and sectional area of the neurons with nucleus in the ventral part (ventral side of the central canal level; which includes roughly laminae VII, VIII and IX of Rexed's [33] of the 5th cervical gray matter) were examined in three K-B-stained 6-μm-thick sections (12-μm apart to avoid double counting of the neurons) on both sides in 11 *kl/kl* and 10 WT mice. Neurons were identified by the presence of Nissl substance and prominent nucleoli. Sectional neuronal area including cytoplasm and nucleus was measured by a digitizer (Measure 5; System Supply, Nagano, Japan). The number of neurons examined was 2,354 in *kl/kl* and 2,110 in WT mice. The frequency distribution of the cell areas by 40-μm^2 increments was obtained. Abercrombie's correction factor [1] was applied for split cell error counting. We defined AHCs here as large neurons with a cell area greater than 400 μm^2, on the basis of their neuronal features and prominent nucleolus in the ventral part of the gray matter.

Measurement of diameter of nucleoli of neurons in the ventral spinal gray matter

Light microscopic black and white pictures of neurons in the ventral spinal gray matter were taken at 200-fold magnification using K-B-stained 5th cervical segments. The film negatives were magnified 19-fold with a microscopy reader RF-3A (Fuji Film corp. Tokyo, Japan) and diameters of the nucleoli on the screen were measured with the ruler of the microscopy reader. In total, 94 neurons in three *kl/kl* and 87 neurons in three WT mice were examined. The frequency distribution by 0.3-μm increments was obtained.

Amount of cytoplasmic RNA in the AHCs

The cytoplasmic RNA content was measured in AHCs with nucleolus by the integrated OD of pyronin Y-stained 6-μm-thick sections. The measurement of the pyronin Y-stained area with an image analyzer has been reported as a reliable method for quantitative assessment of RNA [36]. Integrated OD was measured in the cytoplasm in a routine bright field of Zeiss Axiovert 135 with 12 bits camera (Carl Zeiss, Oberkochen, Germany) using the MetaMorph (Universal Imaging. Co., West Chester, PA, USA) software. Measurement was performed in 100 randomly distributed AHCs with nucleolus in *klotho* and WT mice each (10 AHCs/mouse,10 mice each).

Ultrastructural investigation of the AHCs

Tissue blocks of the 5th cervical cords, fixed with 3% GA-1% PFA in 0.1 M PB, were postfixed with 1% osmium tetroxide, then dehydrated through a graded ethanol series, and embedded in Epon 812. Toluidine blue-stained 1-μm-thick sections were examined using a light microscope, and ultrathin sections of the ventral part of the spinal cords were stained with lead citrate and uranyl acetate and examined using an electron microscope (H9000; Hitachi, Tokyo, Japan) at 100 kV.

Measurement of transcription activity of rRNA gene in neurons in the ventral spinal gray matter

Silver staining of nucleolar organizer region-associated proteins (AgNORs) [4, 6, 14, 18, 19, 21, 30] was used to evaluate the rRNA gene transcription activity in the neurons in the ventral gray matter in *kl/kl* and WT mice. PFA-fixed paraffin-embedded 6-μm-thick sections of the 5th cervical segment 12 μm apart were used for the staining.

Microscopic slides were deparaffinized with xylene, dehydrated in an alcohol series, rinsed with tap water, then stained with a 1:2 blended solution of freshly prepared: (i) 2% gelatin in 1% aqueous formic acid and (ii) 50% silver nitrate solution in deionized and distilled water (DDW). The slides were incubated at 37°C in darkness for 20 min, rinsed in DDW, dehydrated with an alcohol series and xylene, and covered with DPX. Areas of AgNOR-positive regions and the nucleus were examined by a digitizer (System Supply, Nagano, Japan), and the ratio was evaluated. Two hundred thirties neurons from four *kl/kl* and 156 neurons from five WT mice were examined.

Statistical evaluation

Statistical evaluation was performed using the Mann-Whitney U-test to compare the ratio between *kl/kl* and WT mice.

Results

Body and brain weights

The body weight of *kl/kl* mice aged 7 weeks was about one-third that of the WT mice, and the brain weight was about four-fifths of the WT mice (Table 1).

RT-PCR for *klotho* gene expression in the spinal cords

After 40 cycles of RT-PCR, *klotho* gene expression was seen both in WT and in *kl/kl* mice. The expression in *kl/kl* mice was quite weak but significantly positive (Fig. 1). G3PDH was used as control, and the intensities did not differ between *kl/kl* and WT mice. The possibility of DNA contamination as a source of amplified products was believed to be excluded, since the *klotho* gene expression was not seen in the negative control (data not shown).

Light microscopic findings of the central nervous system

The neuronal population and size of neurons in the brains of *kl/kl* mice did not show any apparent differences from those of the controls. The cross-sectional area of the gray and white matter of the cervical and lumbar segments of the spinal cord of *klkl* mice was smaller than that in WT mice, in spite of good preservation of the cross-sectional area (Fig. 2A, B) and the neurons of the posterior horn (Fig. 2C, D) of *kl/kl* mice. Large AHCs were seen more frequently in WT than in the *kl/kl* mice, and small neurons were seen more often in the ventral gray matter in *kl/kl* mice (Fig. 2E, F). In the AHCs of *kl/kl* mice, the amount of Nissl substance,

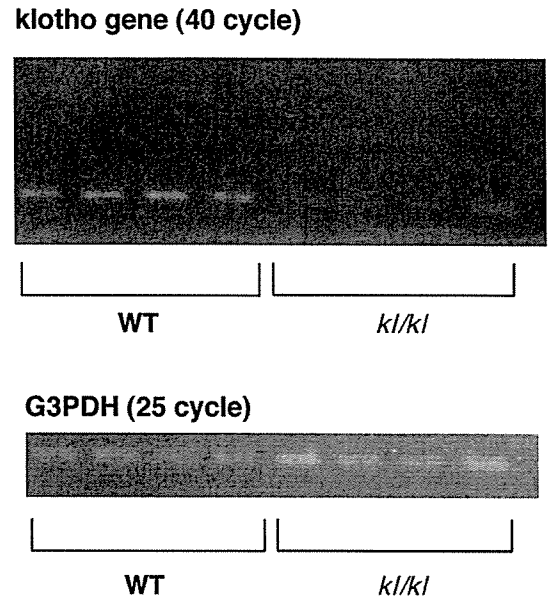

Fig. 1 *Klotho* gene expression by RT-PCR in the spinal cord. After 40 cycles of RT-PCR, *klotho* gene expression was seen in both WT and in *kl/kl* mice. *klotho* gene expression in *kl/kl* mice is quite weak but significant. G3PDH was used as control, and the intensities were not different between the two genotypes (*RT* reverse transcription, *WT* wild-type, *kl/kl* homozygotes with the *klotho* gene mutation)

i.e., rough endoplasmic reticulum (rER), was smaller (chromatolysis) than that in WT mice (Fig. 2G), and slight but evident accumulation of phosphorylated neurofilaments was observed (Fig. 2I, J). GFAP-immunopositive reactive gliosis was seen in the ventral horn of *kl/kl* mice (Fig. 2K, L), and a moderate increase of number of the IB4-positive cells was seen in the anterior horn in *kl/kl* mice; no significant ubiquitin-immunopositive accumulation, Bunina bodies, or spheroids were observed.

Quantitative examination of neurons in the ventral gray matter

There was no significant difference in the number of the neurons in the ventral part of the spinal gray matter between *kl/kl* and WT mice (Fig. 2H). However, the frequency distribution of the sectional area of the neurons in the ventral gray matter of the 5th cervical cord in the 40-μm^2 increments showed one peak at 120 μm^2 in *kl/kl* mice but 160 μm^2 in WT mice, indicating that the neurons in *kl/kl* mice were smaller (Fig. 3A). The number of large neurons with a cross-sectional area over 400 μm^2 was significantly lower in *kl/kl* mice than in WT ($P < 0.0001$) (Fig. 3B). The highest peaks of distribution frequency by 0.3-μm increments of the diameter of nucleoli of neurons in the ventral spinal gray matter were at 2.1–2.4 μm in *kl/kl* mice, but at 2.7–3.0 μm in

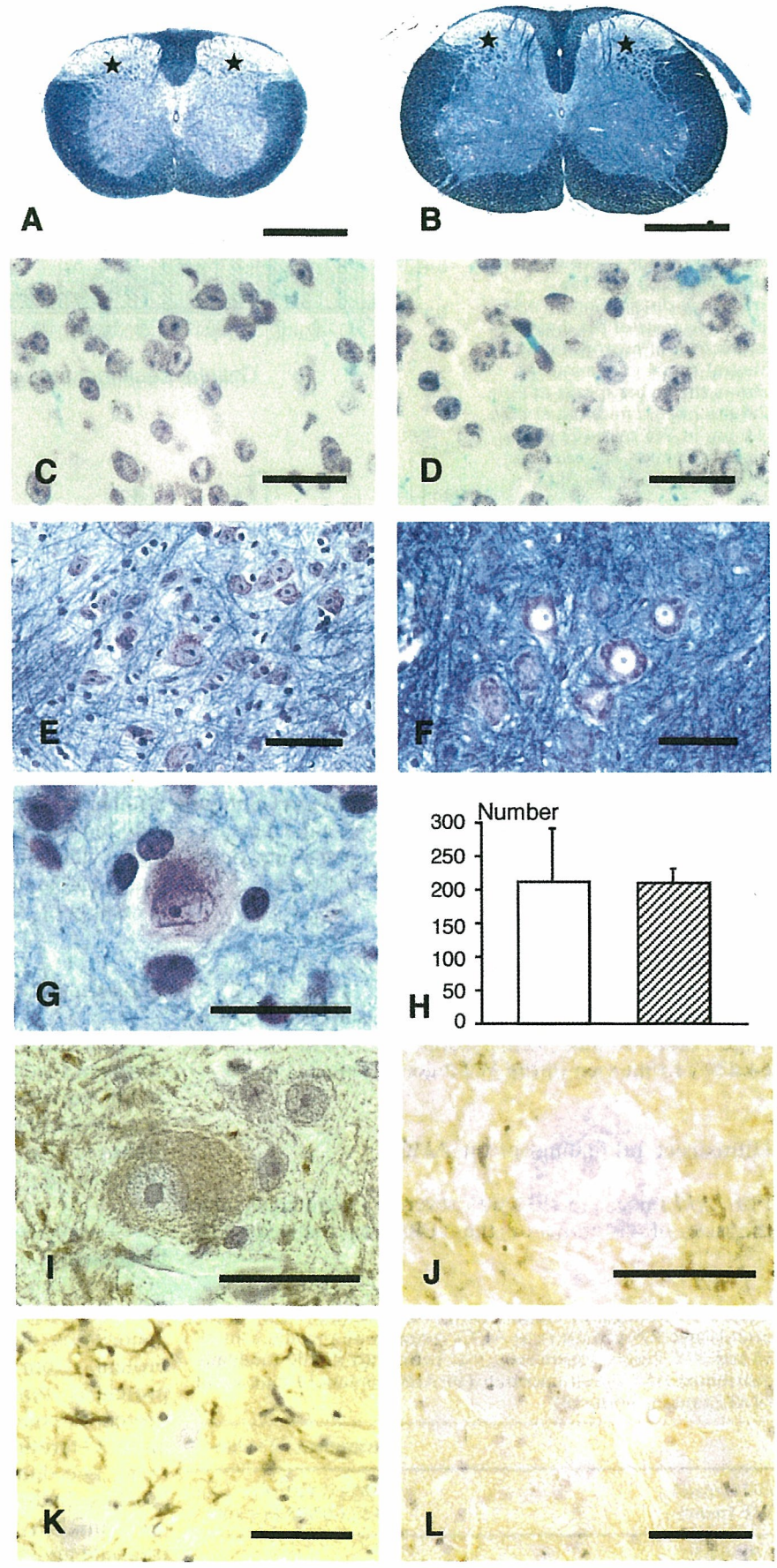

Fig. 2 Light microscopic findings of the 5th cervical spinal cord. Cross-sectional area of the gray and white matter is smaller in *kl/kl* mice (**A**) than in WT mice (**B**), whereas the posterior horn (*asterisk*) is well preserved both in area, size and the number of neurons (**C** *kl/kl* mice, **D** WT mice). Large AHCs are seen more frequently in WT mice (**F**) than in *kl/kl* mice (**E**), and small neurons are seen more frequently in the anterior horn in *kl/kl* mice (**E**) than in WT mice (**F**). The amount of Nissl substance in the AHCs in *kl/kl* mice is less than that in WT mice, indicating chromatolysis by the *klotho* insufficiency (**G**). Accumulation of phosphorylated neurofilaments is observed in the AHCs of *kl/kl* mice (**I**) as compared with the WT mice (**J**). GFAP-immunopositive reactive gliosis is seen in the ventral horn of *kl/kl* mice (**K**) as compared with WT mice (**L**). There is no significant difference in the number of neurons in the ventral part of the spinal gray matter between *kl/kl* mice (*open bar*) and WT mice (*hatched bar*) (*error bars* indicate SD) (**H**) (*AHC* anterior horn cell, *GFAP* glial fibrillary acidic protein). **A–G** Klüver-Barrera staining; **I, J** SMI-31-immunohistochemistry; **K, L** GFAP immunohistochemistry. *Bars* **A, B** 0.5 mm; **C, D, G, I, J** 25 μm; **E, F, K, L** 50 μm

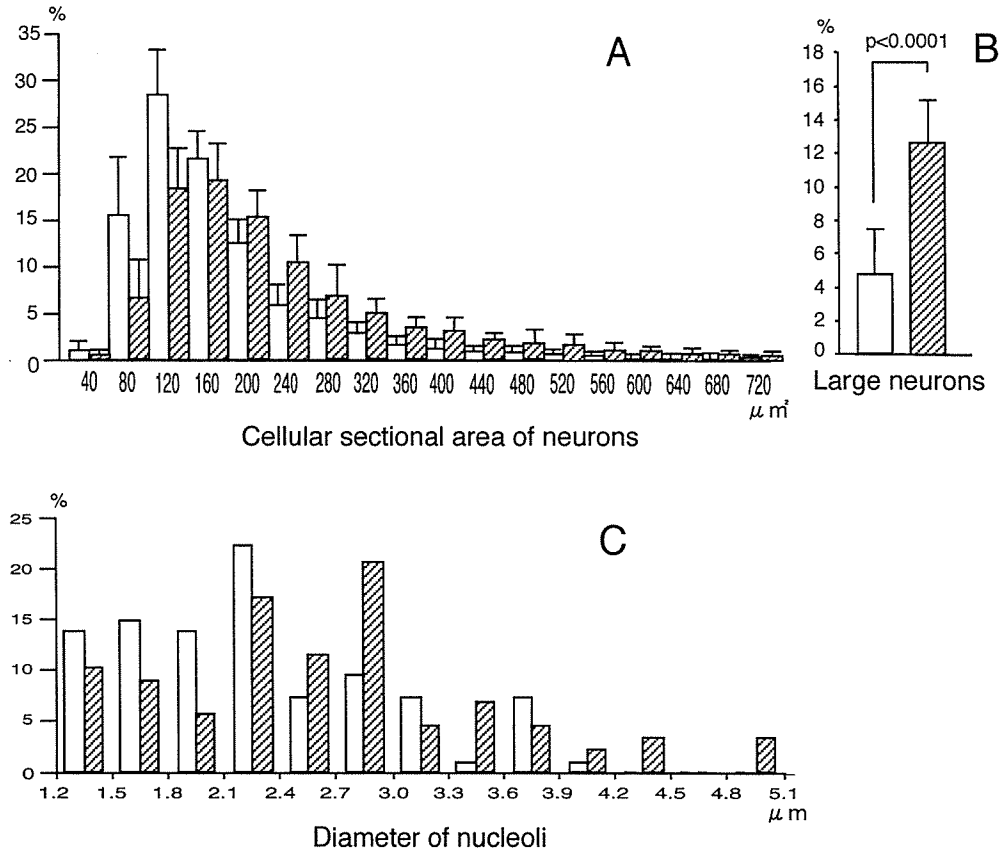

Fig. 3 Distribution of the sectional area of the neurons in the ventral gray matter of the 5th cervical cord. The frequency distribution of the sectional area of the neurons shows one peak at 120 μm^2 in *kl/kl* mice but 160 μm^2 in WT mice, indicating smaller neurons in the *kl/kl* mice (**A**). The number of large neurons with a cross-sectional area over 400 μm^2 is significantly lower in *kl/kl* mice than WT mice (**B**). The frequency distribution by 0.3-μm increments of the diameter of nucleoli of neurons in the ventral spinal gray matter shows the highest peaks at 2.1–2.4 μm in *kl/kl* mice but at 2.7–3.0 μm in WT mice (**C**). *Open bars*: *kl/kl* mice, *hatched bars*: WT mice, *error bars*: SD

WT mice (Fig. 3C). The diameter of neuron nuclei in the ventral spinal gray matter was 2.50 ± 0.91 μm (mean ± SD) in *kl/kl* mice and 2.67 ± 0.77 μm in WT mice; those in *kl/kl* mice were significantly smaller ($P < 0.01$).

Amount of cytoplasmic RNA in AHCs

The integrated OD value of the cytoplasmic RNA in the large AHCs stained with pyronin Y in *kl/kl mice* was 64.4% of that seen in the WT mice (Table 2, Fig. 4).

Ultrastructural findings of the AHCs

For *kl/kl* mice, the rER was severely fragmented, and the size of cisternae of the rER was reduced. The number of the attached and free ribosomes was noticeably reduced in the AHCs as compared to those in WT mice, while mitochondria, nuclear membrane, karyoplasm and nucleolus in the AHCs in these mice appeared normal (Fig. 5A, B).

Table 2 The integrated optical density values (mean ± SD) of the cytoplasmic RNA in the large AHCs stained with pyronin Y in *kl/kl* and WT mice. Measurement was performed in 100 randomly distributed AHCs with nucleolus (10 AHCs/mouse,10 mice each) (*AHC* anterior horn cell)

	Integrated OD value
kl/kl (male)	5,424 ± 3,450* ($n = 100$)
WT (male)	8,427 ± 6,988 ($n = 100$)

*$P < 0.05$

Transcription activity of rRNA gene in the AHCs

AgNOR-positive areas were clearly and exclusively observed in dark fine granules within the nucleus and in the nucleolus. The ratios of AgNOR-positive areas to cross-sectional areas of the nucleus were significantly lower in the neurons of *kl/kl* mice than of WT (Fig. 6A–C).

Discussion

The *klotho* gene carries two varieties of mRNA. The majority is mRNA coding a membrane-type Klotho protein, from which a transmembrane-type Klotho protein is translated [27, 29]. The transmembrane-type protein is composed of an N-terminal signal sequence and a C-terminal transmembrane domain, and between them, two domains (KL1, KL2) homologous to β-glucosidase hydrolyzing steroid β-glucuronides [39]. The other mRNA variety gives rise to strap codons, which translate an approximately half-length secretory Klotho

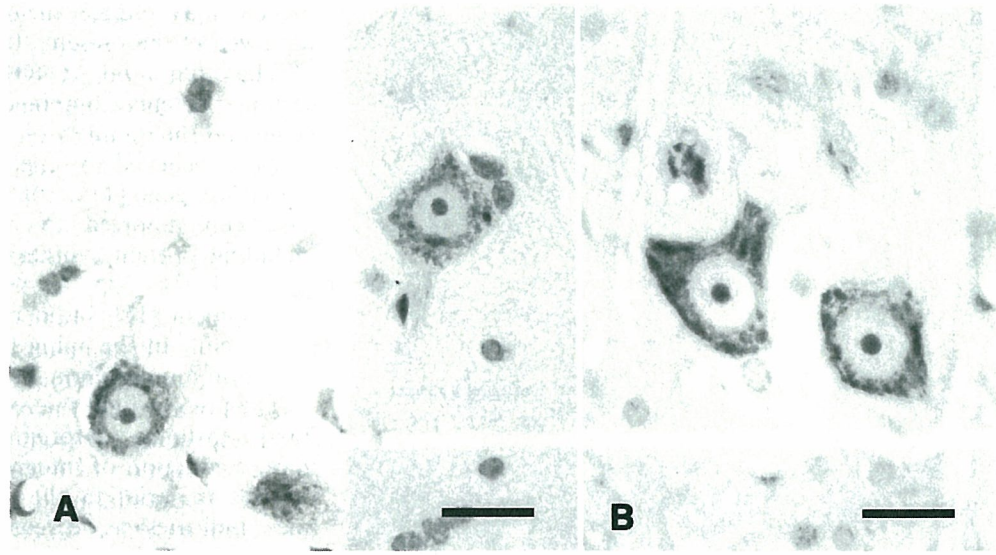

Fig. 4 Pyronin Y-stained AHCs in *kl/kl* (**A**) and WT (**B**) mice. *Bars* 20 μm

protein. The secretory Klotho protein has only a signal sequence and KL1 domain. It is not known whether Klotho proteins have enzymatic activity. The *klotho* gene is reported to be strongly expressed in the kidneys, and weakly in the brain. *Klotho* gene expression has not been reported in the lungs, bones, or skin, which show severe pathological changes in *kl/kl* mice. These facts suggest the possibility that pathological findings in *kl/kl* mice are not a simple phenotype of the *klotho* gene, but that the secretory Klotho protein may have some function whereby pathological changes are suppressed in WT mice [27, 29].

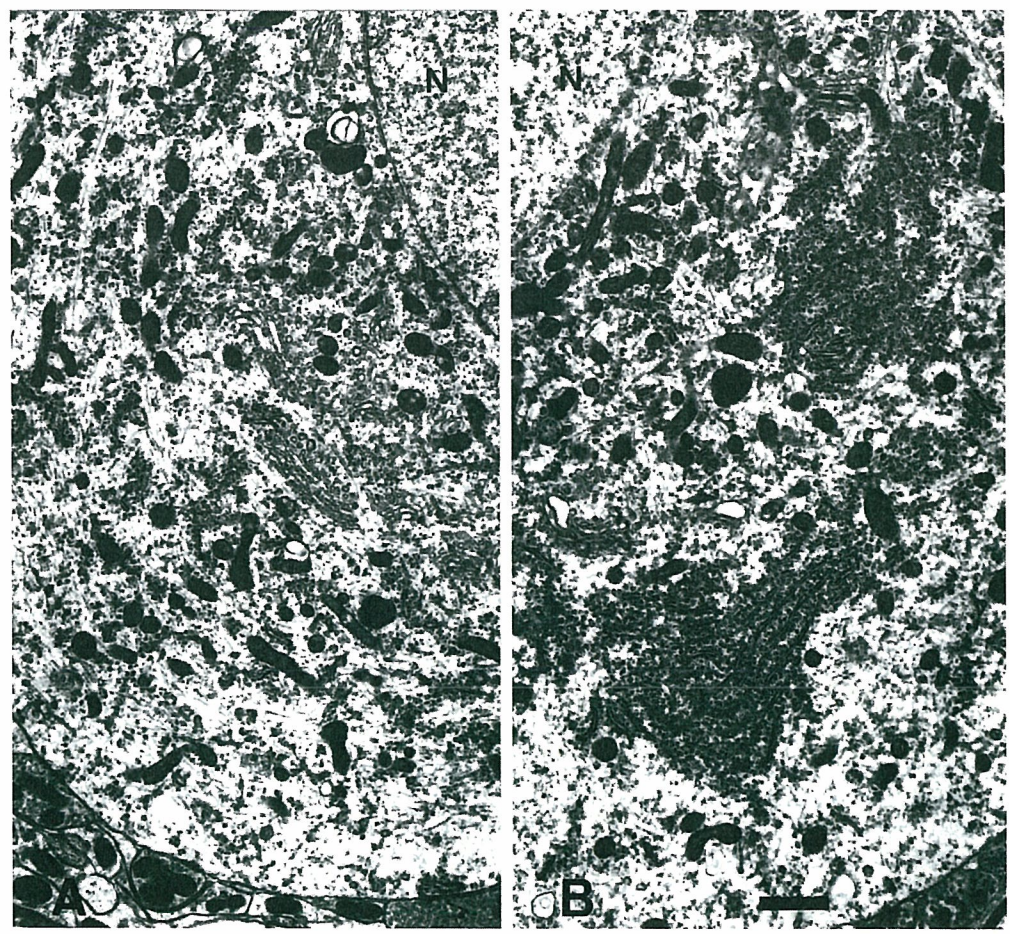

Fig. 5 Ultrastructure of the AHCs. The rERs are severely fragmented, and the amount of rER and the number of free ribosomes sre obviously lower in the neurons of *kl/kl* mice (**A**) as compared with those in WT mice (**B**), whereas mitochondria, nuclear membrane, and nuclear karyoplasm and nucleolus in the AHCs in *kl/kl* mice appear unchanged (*rER* rough endoplasmic reticulum, *N* nucleus). Uranyl-lead staining. *Bar* 1 μm

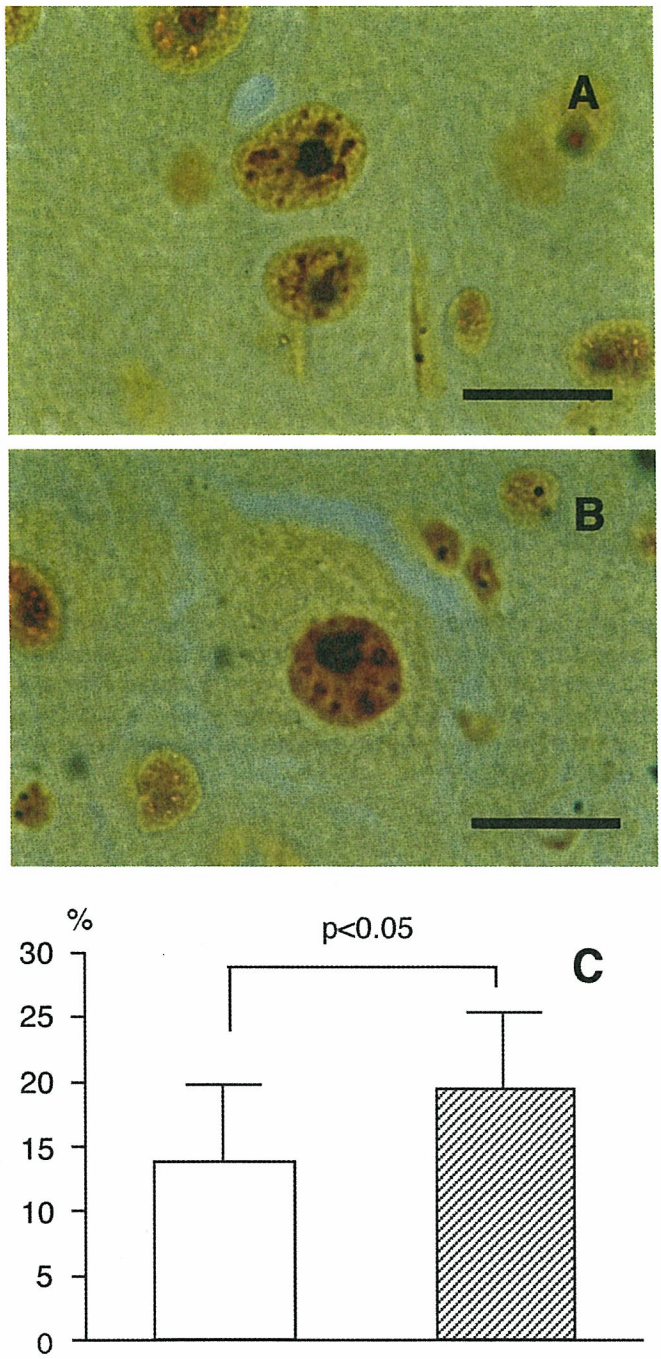

Fig. 6 Transcription activity of rRNA gene in the AHCs. AgNOR-positive area in large AHCs of the *kl/kl* mice (**A**) and WT mice (**B**). The ratio of this area to cross-sectional cellular area of the nucleus is significantly lower in *kl/kl* mice (*open bar*) than WT mice (*hatched bar*) (*error bars* indicate SD) (**C**) (*rRNA* ribosomal RNA, *AgNORs* Silver staining of nucleolar organizer region-associated proteins)

Our present investigation on *klotho* gene expression revealed that the gene was observed strongly in WT and weakly, but significantly, in *kl/kl* mice after 40 cycles in RT-PCR in the spinal cord. This result demonstrates that *kl/kl* mice are not null but severe hypomorph mice of the Klotho protein, and that the decrease of this protein may induce various morphological alterations observed in the present study.

The differential AgNOR staining is believed to stain certain proteins combined specifically with an rRNA gene, and the quantity of the proteins (AgNOR-positive areas) is believed to reflect the transcription activity of the rRNA gene [4, 6, 14]. To date, AgNOR stainability has been reported to be an index of phenomena including protein synthesis [4, 12], tumor proliferation [7, 8, 11, 31, 32, 34, 43], long-term changes during development [12], brain augmentation due to learning [42], decline in the aging brain [22, 23], and age-related reduction among dermal fibroblasts [8, 38].

The present light microscopic study showed a loss of Nissl substance (chromatolysis) in the AHCs of *kl/kl* mice. Reduction of integrated OD value of pyronin Y-positive material in the cytoplasm of AHCs in *kl/kl* mice indicates a decrease of the cytoplasmic RNA content, and ultrastructural investigation of AHCs revealed a reduction of the number of attached and free ribosomes and of rER in the mice in the present study. The ratio between the activity of rRNA gene transcription and the size of the nucleus in the anterior horn cells were evaluated. The results indicated that the depletion of the activity of rRNA gene transcription was not proportional to overall cell size. Thus, decreased transcription activity of the rRNA gene in the spinal neurons observed in the present study may cause a decrease in cytoplasmic RNA, ribosomes and rER of the AHCs. The reduction of the amount of the ribosomes and rER might induce small neurons in the AHCs of the spinal cord with sparing the posterior horn in *kl/kl* mice. To determine the cause and mechanism, the amount of Klotho protein should be examined both in the ventral and posterior horns. In addition, regarding the mechanism of reduction of rRNA gene transcription activity, it should be elucidated whether or not the rRNA gene decreases in the chromosomal DNA; some genes are unavailable in the hybridization after being covered by proteins or other cross-linkers [13], and the RNA polymerase I, TFIIA, TFIIB, TATA box-binding protein, and CRE-binding protein exist normally in the AHCs [2].

A decreased number of small neurons and the absence of chromatolysis have been reported in the AHCs of aged humans [5, 26, 37, 40]. These findings differ from those observed in the *kl/kl* mice in the present study. Thus, the pathological mechanisms occurring in the spinal cord in aged humans and *kl/kl* mice are considered to be basically dissimilar. Further examination of the spinal cords in fetus and newborn, to analyze possibly overlapping developmental disturbance, is needed to determine the cause of the severe reduction in the volume of the spinal cord in *kl/kl* mice.

Kl/kl mice show a marked reduction in body weight. Thus, developmental retardation may exist in the mice. However, the brain is relatively well developed and preserved. Neuronal population and the size of neurons in the brains did not show any apparent differences from